Supra-molecular agents running tasks intelligently (SMARTI): recent developments in molecular logic-based computation

MSDE

ROYAL SOCIETY OF CHEMISTRY

REVIEW

Cite this: *Mol. Syst. Des. Eng.*, 2020, **5**, 1325

Supra-molecular agents running tasks intelligently (SMARTI): recent developments in molecular logic-based computation†

Chao-Yi Yao, Hong-Yu Lin, Hannah S. N. Crory and A. Prasanna de Silva

Received 20th June 2020,
Accepted 1st September 2020

DOI: 10.1039/d0me00082e

rsc.li/molecular-engineering

The field of molecular information handling and processing from a Boolean starting point has grown strongly during the past five years to make important contributions to the areas of intracellular computation, delivery of functional species and information security. Additionally, there has been consolidation of the original avenue of multi-input sensing devices, besides contributions to complex, multivalued and reconfigurable logic systems. Small supramolecules form the majority of these devices, though there is a strong showing from DNA and protein devices operating in a supramolecular fashion. These devices serve as our agents to perform intelligent functions which we cannot do, such as within living cells. The design and engineering of supramolecular systems is responsible for the origin of molecular logic-based computation and for its longevity.

Design, System, Application

The modular 'fluorophore–spacer–receptor' system is a natural approach to designing supramolecular switches with chemical inputs and light output which can operate in small spaces. Extensions with additional spacer and receptor modules permit more complex input–output profiles as found in computer hardware. Some aspects of software engineering can also be emulated in this way. From this starting point, various (bio) molecular mechanisms have been co-opted to build a range of logic-based computing systems. These have applications in sensing and delivery with a degree of intelligence.

1. Introduction to molecular design and engineering aspects of logic systems

Chemistry is not renowned for systems based on engineering designs. Engineers are accustomed to designing their systems according to long-established principles. Then, such

School of Chemistry and Chemical Engineering, Queen's University, Belfast BT9 5AG, Northern Ireland, UK. E-mail: a.desilva@qub.ac.uk

† Electronic supplementary information (ESI) available: List of sources of molecular logic devices and cases which are understandable as such. List of sources of sensors/switches designed or understood on the basis of competing fluorescence and PET. See DOI: 10.1039/d0me00082e

Hongyu Lin, Hannah Crory , Chaoyi Yao and AP de Silva

Has anyone not heard of the 'Titanic'? The famous ship was constructed in the Harland & Wolff shipyard in the background of the photograph. Belfast in Northern Ireland was world-renowned for its shipbuilding and its mechanical systems design and engineering. It is molecular systems design and engineering that has brought the four co-authors to Belfast from different corners of the world. Hongyu Lin is from Yushan, Jiangxi province, P. R. China, Hannah Crory commutes from Banbridge, Northern Ireland, Chaoyi Yao hails from Jingzhou, Hubei province, P. R. China and AP de Silva is a native of Colombo, Sri Lanka. Too bad about the iceberg…Photo by Michael Bingham.

knowledge passes from science across to engineering, at least in the popular imagination. For instance, knowledge about static structures which were gathered by natural philosophers several millennia ago is now the foundation of civil engineering institutions. Numerical calculations are *de rigueur* in engineering designs. Engineers are also used to working with systems they can see, with optical microscopes at worst. Another part of the engineering gospel is modularity, where components are assembled so that the system achieves its end-result which the components cannot. The components themselves may serve within different systems because of their predictive properties.

On the other hand, chemists work with molecule-based systems which are invisible except under the most sensitive scanning probe microscopes. Hence, ancient knowledge of medicinal plants, for instance, was not generally incorporated into the chemical canon at a molecular level until the 20th century. Systems chemistry is a very recent entrant and emergence as a concept is only encountered in regular chemical discourse in the 21st century[1] (even though it was recognized for over two centuries that molecules express properties unseen in their constituent atoms). Around the 1980's, we[2] and others[3–11] came across small supramolecular systems[12,13] which expressed chemically-switchable fluorescence whereas their components did not. The chemical input-light output nature[14–27] of these systems in a computer- or civil-engineering sense was recognized before too long. Also, these components could show modular behaviour. Furthermore, principles[28] (albeit established only two decades previously) could be employed to make quantitative calculations to predict much of the system properties. These systems have now grown into molecular sensors[29–35] and logic-based computing devices.[14–27,36] The latter can now be understood to have contributions from at least 1104 laboratories worldwide (Fig. 1 and Table S1†). We have here molecular systems designed from an engineering perspective, which are particularly suited for discussion in this journal.

To illustrate these ideas, we feature **1** (ref. 37) which switches fluorescence 'off' at 'high' H^+ concentration ($10^{-2.5}$ M) and 'on' at 'low' H^+ concentration (10^{-7} M). In Boolean terms, this is a NOT logic gate[38] with H^+ input and fluorescence output.[15] The fluorophore component of **1** can be spotted in a control compound **2** which is a known optical whitener[39,40] absorbing at 359 nm (λ_{abs}) with an extinction coefficient (ε) of 22 000 M^{-1} cm^{-1} and emitting at 475 nm (λ_{flu}) with a pH-independent quantum yield (ϕ) of 0.19 in methanol : water (1 : 4).

When switched 'on', **1** gives λ_{abs} = 359, ε = 22 000, λ_{flu} = 475, ϕ = 0.13 in the same units and in the same solvent. ϕ values are notoriously hard to predict so the degree of agreement here is reasonable, but the other parameters are predicted within experimental error. The H^+-sensitivity of **1** arises from its 4-substituted benzoate moiety. Being a weak Brønsted acid, 4-methylbenzoic acid has an acid dissociation constant (pK_a) of 4.5. This is identical to the base association

Fig. 1 Approximate world maps of the sources of molecular logic devices and cases which are understandable as such. Only the names of corresponding authors from the literature are given. The simplest cases based on single-input and single-output are not shown. A more detailed list (surname, initials, city, institute) is given in ESI† (Table S1).

constant ($\log\beta_{H^+}$) of the conjugate base 4-methylbenzoate. **1** switches its fluorescence 'on/off' at pH = 4.2. It is also gratifying that **1**'s pK_a value is found by pH-dependent solubility measurements to be 4.4. When switched 'off', **1** gives ϕ = 0.003. Another control compound, methyl benzoate ester **3** corresponds to the 'off' fluorescent state of **1**. **3** has λ_{abs} = 359, ε = 22 000, λ_{flu} = 475, ϕ = 0.003. Such use of control compounds to quantitatively mirror the 'on' and 'off' states of a 'on–off' switchable system[41] strengthens its design.

The principle underpinning **1**'s switching behaviour is photoinduced electron transfer (PET) sensing/switching,[29–35] which is based on the even stronger principle of PET

Fig. 2 Approximate world maps of sources of sensors/switches designed or understood on the basis of competing fluorescence and PET. Only the names of corresponding authors from the literature are given. A more detailed list (surname, initials, city, institute) is given in ESI† (Table S2).

itself.[28,42] We have found that PET-based fluorescence sensing/switching has been employed as a design by at least 912 laboratories worldwide (Fig. 2 and Table S2†). In the 'off' fluorescent state of **1**, PET out-competes fluorescence for the deactivation of the excited state, whereas PET loses out in the 'on' fluorescent state. The thermodynamic feasibility of PET for **1**.H$^+$ is given by the Weller eqn (1),[28] where the last term (−0.1) represents the approximate pairing energy between the fluorophore radical cation and the receptor radical anion in a polar medium. As such, the term is solvent-dependent and leads to sensors for polarity.[43] The excited state energy is described in terms of redox potentials by eqn (2).[44]

$$\Delta G_{PET} = -E_{ex\ fluorophore} + E_{ox\ fluorophore} - E_{red\ receptor.H^+} - 0.1 \quad (1)$$

and

$$E_{ex\ fluorophore} = E_{ox\ fluorophore} - E_{red\ fluorophore} \quad (2)$$

where $E_{ex\ fluorophore}$ is excited state energy of the fluorophore, $E_{ox\ fluorophore}$ is the oxidation potential of the fluorophore, $E_{red\ fluorophore}$ is the reduction potential of the fluorophore (−2.3 V *vs.* sce)[45] and $E_{red\ receptor.H^+}$ is the reduction potential of the benzoic acid (−2.2 V *vs.* sce).[46] Since ΔG_{PET} = −0.2 eV, the feasibility of PET is demonstrated. Under such conditions, the rate of PET is likely to be high,[47] and higher than the fluorescence rate. On the other hand, $\Delta G_{PET} > 0$ for unprotonated **1**, since it is likely[44] that $E_{red\ receptor} < -2.5$ eV, and so PET will not be thermodynamically feasible.

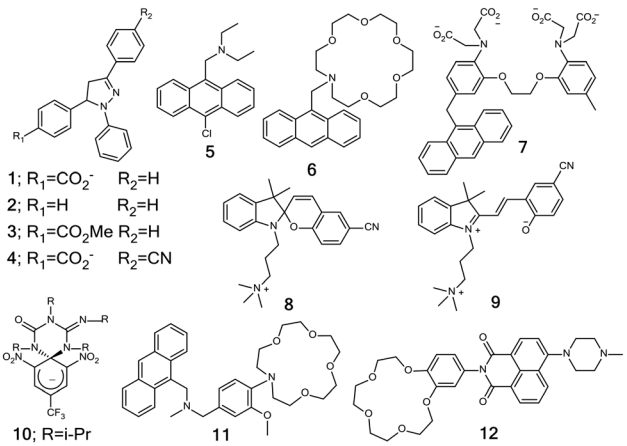

If ΔG_{PET} is calculated from frontier orbital energies rather than being determined from experimental quantities as done above, it appears that values of up to +0.6 eV can still lead to PET having higher rates than those of fluorescence.[48] So it is clear that the H$^+$-induced fluorescence switching of **1** in a NOT logical manner is essentially completely predictable according to engineering practice as applied to molecules. Our confidence in such an engineering design is increased further by calculating ΔG_{PET} similarly for **4**.H$^+$ to be +0.9 eV and then finding that **4** switches its fluorescence hardly at all under the influence of H$^+$.

The modular behaviour of **1** discussed above is due to the spacer component which isolates the fluorophore from the receptor and *vice versa*, except for the relatively long-range process of PET which leads to the emergent property of NOT logic action. Such 'fluorophore–spacer–receptor' formats create system behaviour at a small scale. The supramolecular nature of such connected components has been pointed out previously.[13] The positioning of a receptor not too far but not too close from a fluorophore in **1** has similarities with the placement of substituents at a

reasonable distance from a reactive site in the study of substituent effects in physical organic chemistry.[49,50] More complex logic functions such as 'off–on–off'[51] and INHIBIT[52] are produced by derivatizing **1** or **2** within the 'fluorophore–spacer–receptor' frame of reference.

'Fluorophore–spacer–receptor' systems can also produce YES logic gates[15] when PET is arranged to occur in the guest-free receptor state[53] according to eqn (1) and (2), *e.g.* **5** showing fluorescence output with H^+ input.[2,54] However, the $\log\beta_{H^+}$ value of the component amine is not carried across to **5** owing to the influence of the bulky fluorophore across the short methylene spacer in causing steric hindrance to solvation of the guest-bound receptor. When a larger receptor is employed to accommodate K^+ input into **6**,[10] the centre of such a receptor is rather remote from the fluorophore in spite of the short spacer and so the steric hindrance to solvation is negligible. Modularity is restored as judged by the similarity of $\log\beta_{K^+}$ values of **6** and its component azacrown ether. $\log\beta_{Ca^{2+}}$ values of **7** and its component amino acid receptor are also in close agreement.[55]

Modularity can be exploited further to build up logic systems in a stepwise manner. A fluorophore on its own would serve as a PASS 1 logic gate,[15] whereas 'fluorophore–spacer–receptor' systems give rise to YES and NOT gates when appropriate PET-active modules are chosen. The use of a non-selective receptor within these create OR[56] or NOR[57] logic. Expansion to 'fluorophore–spacer$_1$–receptor$_1$–spacer$_2$–receptor$_2$' and 'fluorophore–spacer$_1$–receptor$_1$–spacer$_2$–receptor$_2$–spacer$_3$–receptor$_3$' systems produce 2-input[14] and 3-input AND[58] logic gates respectively. Fig. 3 schematizes this build-up. In this way, supramolecular agents of increasing intelligence can be introduced to run tasks on our behalf and SMARTI starts to happen. Indeed, such stepwise build-up of supramolecular agents can even be performed by noncovalent assembly routines.[59]

Now that the engineering foundations of molecular logic systems have been outlined, the following sections will expand on modern developments along some of the most intensively studied lines in this field.

2. Logic elements and 2/3-input systems

This section starts off with two components of logic gates – triodes and transistors – to illustrate how chemists' emulation of logic gates even reaches down to their guts. Then we showcase

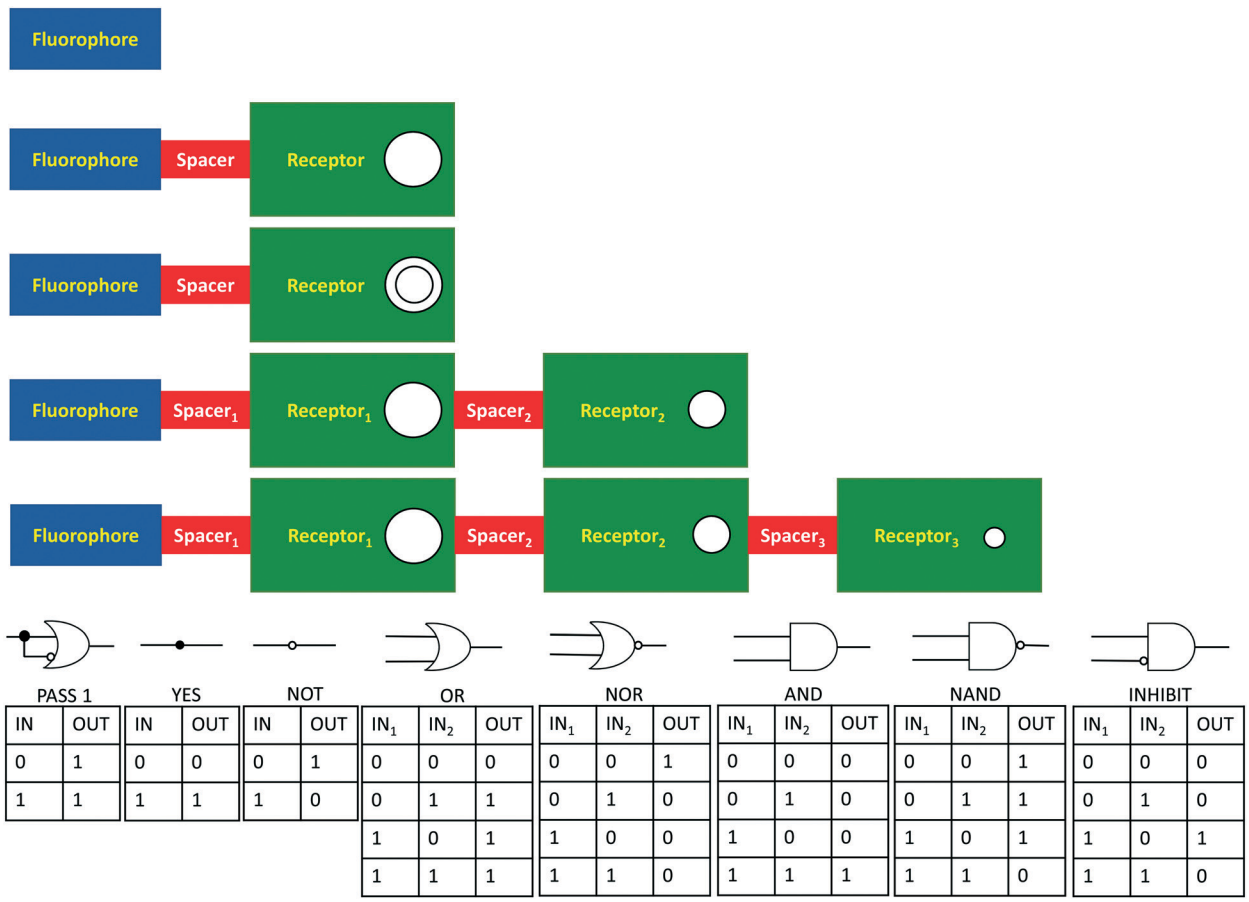

PASS 1		YES		NOT		OR			NOR			AND			NAND			INHIBIT		
IN	OUT	IN	OUT	IN	OUT	IN_1	IN_2	OUT	IN_1	IN_2	OUT	IN_1	IN_2	OUT	IN_1	IN_2	OUT	IN_1	IN_2	OUT
0	1	0	0	0	1	0	0	0	0	0	1	0	0	0	0	0	1	0	0	0
1	1	1	1	1	0	0	1	1	0	1	0	0	1	0	0	1	1	0	1	0
						1	0	1	1	0	0	1	0	0	1	0	1	1	0	1
						1	1	1	1	1	0	1	1	1	1	1	0	1	1	0

Fig. 3 Build-up of logic gates by incrementing modules. Fluorophore = PASS 1; fluorophore–spacer–receptor = YES or NOT; fluorophore–spacer–nonselective receptor = OR or NOR; fluorophore–spacer$_1$–receptor$_1$–spacer$_2$–receptor$_2$ = 2-input AND or NAND or INHIBIT; fluorophore–spacer$_1$–receptor$_1$–spacer$_2$–receptor$_2$–spacer$_3$–receptor$_3$ = 3-input AND. Physical electronic representations of these logic gates are shown, along with their truth tables, except for 3-input AND which is described later in Fig. 7. See text for molecular implementations of PASS 1 (derivative of **50**), YES (**50**), NOT (**1**), OR (**27**), NOR(**24**), AND (**11**), NAND (**65**) and INHIBIT (**22**/**23**) gates.

the strength of diversity present in molecular logic. Outputs consisting of absorbance, fluorescence, luminescence, electrical conductivity, single molecule conductance and product formation are discussed. Simple chemical species, biospecies (*e.g.* enzymes) and physical entities (light dose, temperature) serve as inputs. As specified in the title, the devices are supermolecules of various kinds, along with some nanoparticle and bulk material constructs carrying supramolecular attributes. Recent logic types that caught our eye are AND, INHIBIT and NOR gates (Fig. 3). The dominance of AND gates here mirrors the state of the field at least from a chemical viewpoint, a situation which existed from the very beginnings of the field.[14] Their popularity is also due to the selectivity built into AND logic, where two (or more) individuals are needed to produce the outcome. Not only have such selectivity (when applied to words) sharpened internet search engines but selectivity is also the hallmark of (bio) chemical reactivity and analysis. AND logic is also critical for direct detection of congregations of species. Intracellular versions of this are particularly critical and will be taken up in section 9. These illustrate the general point that molecular logic gates can be practically useful problem-solvers without being logically complex. Molecular biology situations which escape the AND monopoly will appear mainly in section 8. The operating principles of a good number of these gates will follow on from section 1 in terms of the fluorescence-PET competition.[29–31] We will endeavour to sketch out the functioning of other gates within the space limits of each paragraph.

Although it is true to say that that logic gates are the workhorses of the information technology revolution, the gates themselves are constructed from semiconductor-based transistors.[60] The predecessors of transistors were the vacuum tube-based triodes.[60] As their name suggests, they are three-electrode devices composed of a cathode and an anode with an intervening grid. Their current output – voltage input curves arising between the cathode and the anode are tunable along the voltage axis by a voltage input applied to the grid. Such tunability of an input–output characteristic can also be arranged within molecular devices.[61–65] A water-soluble spiropyran photochromic[66] **8** (ref. 67) gives rise to the coloured zwitterionic product **9** when irradiated with a sufficiently large dose of 254 nm light but the two states equilibrate significantly even in the dark. The concentration of **9** is pH-dependent in a sigmoidal manner[68] owing to protonation[69] of the phenolate moiety.[70] However under 254 nm irradiation, protonated **9** also cyclizes to give **8** at moderate pH values so that the concentration of **9** is suppressed noticeably. This produces a sigmoidal curve shifted towards basic pH. By controlling the 254 nm light dose, the extent of this curve shift can be manipulated reminiscent of a triode being tuned.

Transistors themselves can be emulated with molecular systems.[71–74] **10** (ref. 74) is protonated on the guanidine upon electrooxidation in acetonitrile to produce an enhanced fluorescence. Electroreduction reverses the situation. A PET process from the guanidine to the cyclohexadiene fluorophore is implicated. Additionally, cooling causes the 'on' state to increase its fluorescence signal by stabilizing the oxidation products *vis-à-vis* **10**. Thus, the fluorescence-potential curve is tuned towards higher fluorescence intensity by decreasing temperature. Field effect transistors, which carry source and drain electrodes with an intervening gate electrode, show an analogous behaviour where the source-drain current–voltage curve is tuned by source-gate voltage.[60] A similar electrode configuration is arranged for **10** by sandwiching a thin film of it in an involatile solvent between electrically conducting glass and normal glass, with the latter containing an auxiliary electrode and a reference electrode.

A two-input AND logic gate would arise if some output is triggered only by the simultaneous presence of two inputs. **11** (ref. 75) is a case based on the classical 'fluorophore–spacer$_1$–receptor$_1$–spacer$_2$–receptor$_2$' system[14] (Fig. 3) where the lodging of H^+ at an aliphatic amine and Na^+ in a *N*-arylaza-15-crown-5 ether stop each of the receptors from serving as PET donors to the anthracene fluorophore. Thus, fluorescence output becomes switched 'on'. The 'high' level of H^+ needs to be controlled to avoid protonation of the azacrown ether. In which case, TRANSFER(H^+) logic would be the result. In contrast, **12** (ref. 76) is a 'receptor$_1$–spacer$_1$–fluorophore–spacer$_2$–receptor$_2$' system[77] (related to Fig. 3) where the fluorescence output displays reasonable Na^+, H^+-driven AND logic behaviour although PET to an aminonaphthalimide fluorophore from a benzocrown ether receptor is endergonic,[78] perhaps because of the short C_0 spacer$_1$. As an aside, this case has enhanced Na^+ binding due to lariat action[79] of the imide carbonyl oxygen.

Instead of fluorescence, luminescence is the output in the case of **13**.[80] This is a common antibacterial drug which chelates Eu^{3+} so that a sensitized luminescence emission[81,82] can potentially occur when the pi-electron system is excited by 347 nm light.[80] However, such emission can be prevented by a PET process from the amine unit which lies just outside the pi-electron system, which in turn, can be prevented by the amine binding to another cation.[83,84] Ag^+ performs this function on the **13**-Eu^{3+} complex, but the luminescence is not emitted until SCN^- is also introduced. Thus, the emission is driven by Ag^+ and SCN^- inputs in an AND logical fashion. The function of SCN^- appears to be the displacement of water molecules in the first coordination shell of Eu^{3+} so that the energy-sapping OH oscillators[81,82] disappear.[85]

AND logic gates driven by two-or higher numbers of inputs can be straightforward determinants of the coincidence of species in space–time by delivering a 'high' light signal.[14,58] This is valuable for directly visualizing such congregations[58] in medically crucial situations. For instance, glutamate is a critical neurotransmitter in the brain, which is delivered along with Zn^{2+} within secretory granules. Detecting glutamate and Zn^{2+} together should image activity in such granules with low backgrounds.[86] **14** forms an imine **15** with glutamate which tightly complexes Zn^{2+} by including an important 5-membered ring containing the imine plus the α-carboxylate. Freezing of the imine bond rotation in the excited state, destabilization of imine non-bonded electrons, rigidification of the pi-system lead to substantial enhancement of fluorescence. On the other hand, **14** is only moderately emissive due to rather low-energy non-bonded electrons on the aldehyde.[87]

Even two enzymes can serve as inputs to an AND gate[88] instead of two small ions. However, when catalysed reactions take place the system loses chemical reversibility. Still, single-use logic systems are valuable in disease diagnosis.[58] The first input, pig liver esterase, hydrolyzes the acetoxy group of **16** which then self-immolates[89] by eliminating a quinonemethide followed by CO_2. The intermediate **17** is produced, which is then acted upon by the second input, nitroreductase, to form **18** *via* loss of a quinoneimine methide. **18** cyclizes to **19** *via* nucleophilic attack on a nitrile group. The emissive form of **19** is the phenolate[90] which is a push–pull pi-system.[91] Changing the sequence of input addition causes a significant loss of the fluorescence output but this is likely to be repaired in subsequent iterations of this type of logic gate.

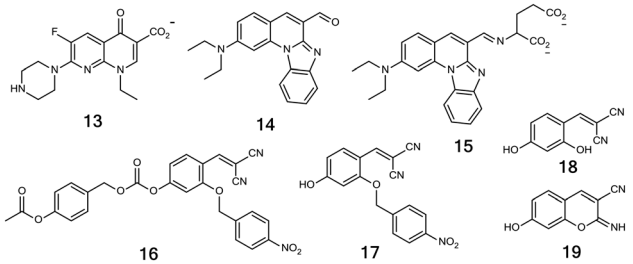

Hydrogen-bonding between secondary ammoniums and benzo-24-crown-8 ethers is the key interaction in the rotaxane of the daisy-chain[92] variety, **20**.[93] Its triarylamine stoppers and the linking amides permit a supramolecular polymerization aided by a PET process between the electron-rich stopper and chloroform solvent. This polymer, which is held together by a triarylamine stack with some photogenerated holes, along with hydrogen-bonding between amide units,[94] leads to fibres. The fibre formation can be considered as the output which arises in an AND logical fashion from the two inputs of light dose and H^+ because removal of the latter dismantles the complexation within the benzo-18-crown-8 ether. However, the mechanically-bonded components move apart akin to a molecular muscle[95] until the triazolium moieties are within the crown cavity so that the stopper-amide segments are sterically prevented from supramolecular polymerization by the crown.

Systems chemistry[1] is fertile ground for multi-stimulus responses of networks.[96] AND logic gate behaviour can be recognized within the self-assembly of components into rather sophisticated structures requiring considerable error-correction and hence, editing time. **21** is composed of three Zn^{2+} centres and three ligands.[97] However, the application of triethylamine as a base ($input_1$) and the provision of ClO_4^- ($input_2$) as a template results in a slow rearrangement to a new system composed of nine Zn^{2+} centres, six hydroxo bridges and five ligands, along with four template ions lying in a chiral groove. Here, the logical output is the formation of the product assembly itself.[98]

Cyclophane **22**/**23** (ref. 99) contains two orthogonal pi-systems, where the smaller unit contains a pyridine which can be protonated reversibly. The longer pi-system can be reversibly photoswitched between the non-planar 'open' and the planar 'closed' forms[100] where the latter has the longest pi-system of all. When connected to a gold substrate and a gold scanning tunnelling microscope tip *via* the sulfur termini of **22**/**23**, its conductance can be measured. The 'high' conductance output is found when the cyclophane is in the 'closed' form produced by a light dose input at 310 nm by an electrocyclic reaction. However, the conductance falls if the pyridine unit is protonated since the HOMO of the longer pi-system is lowered so that it is no longer in resonance with Fermi levels of the electrodes.[101] Indeed, then the LUMO starts to couple to the metal levels but since it is localized on the orthogonal smaller pi-system, the charge transport has to tunnel across less efficiently by this alternate route. As such, this behaviour fits INHIBIT logic (Fig. 3), with H^+ being the inhibiting input. A complication is that the conductance also falls if the 'open' form is produced by 530 nm input (which is needed for resetting purposes anyway). A related case driven by an electrochemical voltage and a UV light dose is also available.[102] Simple photochromics have been understood as light-driven flip-flops with absorbance output,[103] although it should be noted that this idea was specifically discussed by Kuhn during his pioneering experiments.[104] Their logic behaviour when stimulated with H^+ has also been analysed under conditions where the memory aspects are ignored.[69]

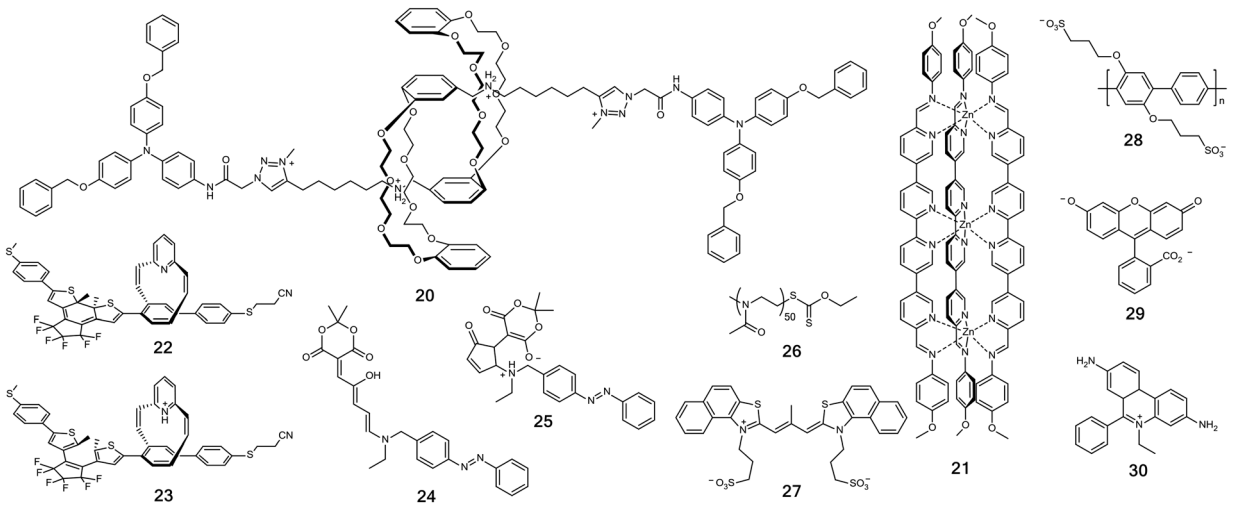

The combination of two photochromic units is also a useful approach to logic device construction,[105–107] especially when the interrogation wavelengths for the forward and backward steps of each unit are well-separated.[106,107] In **24**,[107] the venerable azobenzene moiety is combined with a more recently-discovered donor–acceptor system.[108] The latter unit absorbs a dose of 525 nm light ($input_1$) to convert to a colourless ring-closed version **25**. The output, absorbance at 545 nm, is 'high' for **24** but 'low' for **25**. A dose of 430 nm light ($input_2$) is mainly absorbed by the azobenzene unit in its *E*-form to convert to the *Z*-form but this only alters the absorbance at wavelengths away from where the absorbance is being monitored for logic purposes. However, when applied to **24** as the device, this act appears to allow the azobenzene to photosensitize the ring-closing of the donor–acceptor system so that the output drops to 'low'. If both inputs are applied simultaneously, the presence of the 525 nm light dose ensures that the donor–acceptor system cannot survive in its ring-opened form and reverts to the colourless **25**. We have NOR logic (Fig. 3) as a result.

Au nanoparticles star in a 2-input AND gate[109] by exploiting the red-shift of their plasmon resonance band arising upon their aggregation.[110] Some of the citrate caps on Au nanoparticles are replaced with **26**, where **26** possesses a random coil-to-globule transition at higher temperatures. Such transitions are known for certain poly(acrylamides)[111,112] and some of these have been employed in thermally-driven logic gates.[113] At low temperatures (<22 C) the random coil form of **26** gives rise to polymer brushes which sterically prevents nanoparticle aggregation. At higher temperatures, the collapse of **26** brushes can permit nanoparticle aggregation if the electrostatic repulsion of the citrate caps can be screened by use of 0.05 M NaCl. Thus, temperature and NaCl are the inputs and the absorbance at ~700 nm shows clear AND logic behaviour. This example builds upon one[114] of two prior cases,[114,115] where the citrate caps on Au nanoparticles bind to an Hg^{2+} input species. Guanidinium units of an arginine input species bind to the citrate caps as well. The free valencies of Hg^{2+} can be employed to connect to the amino acid unit of arginine to provide a means of cross-linking and aggregating the Au nanoparticles, which in turn will change the plasmon resonance band from 520 nm to 650 nm. If the output signal is taken as the absorbance at 650 nm, AND logic behaviour emerges.

Although this review is focussed on supramolecular agents, it is important to mention logic devices constructed of bulk materials other than those employed in conventional computation. For instance, bubbles,[116] microelectrodes,[117,118] microelectrochemical cells,[119] waves in media,[120] slime moulds[121] have all been put to use. In the case under discussion, a small electrically-conducting object is placed in an electric field so that a potential difference is induced between its termini. This allows water electrolysis to occur, liberating H_2 and O_2 at the appropriate terminal. The object here is p-type silicon (with hydrogen surface atoms) paired with platinum metal. Silicon requires blue illumination before it becomes conducting. Thus light becomes an input, while the voltage creating the electric field is the other input. The gas evolution (or the current arising during it) serves as the output.[122] In the simplest case, light is necessary and a sufficiently large voltage must feed the electric field if the output is to be 'high', *i.e.* AND logic.

3. Reconfigurable systems

Molecular-logic based computation allows the changing of logic type by changing inputs and outputs[15] – a trick barred to semiconductor-based counterparts. A short section on this topic follows. Chemically-induced band shifts in absorption and emission serve as the operating principle of **27**. The case involving **28–30** works on the basis of electronic energy transfer (EET) between pi-systems. The entry-level gates arising are fully explained within the paragraphs. Some of the more complex gate arrays that result from these principles are summarized as figures so that the scope of the method can be appreciated at a glance. This policy will be followed throughout the review.

The diversity of chemical systems permits the use of various inputs and outputs in molecular logic devices, which means that logic types can be reconfigured in various ways by exploiting input–output heterogeneity.

Cyanine dye **27** can exist as dimer, J (slipped stack)- or H (stack)- aggregate depending on the K^+ concentration or on the pH value in aqueous solution.[123] Each of these states possesses a distinguishable absorption band. So, K^+, H^+-driven logic gates can be constructed. For instance, moderate K^+ and high H^+ concentrations both result in J-aggregates absorbing at 655 nm which represents K^+, H^+-driven OR logic (Fig. 3). If device **27** is complemented with a guanine-rich DNA oligonucleotide to form a G-quadruplex secondary structure in high [K^+], even the monomer state of **27** is observed at 575 nm when it is included in this folded DNA structure. Duplex DNA cannot perform this inclusion. **27** monomer is also fluorescent, which opens another output channel to operate in parallel with the absorbance channel to produce a half-adder (Fig. 4). Similar parallel running of gates was used in the first half-adder in 2000.[124] A cytosine-rich DNA oligonucleotide (the complementary strand to the G-rich oligo) to form an i-motif secondary structure in acid solution can also be added to **27**. The availability of a significant number of aggregation states even allows the construction of a 2-to-4 decoder (Fig. 5) with clear 'on' and 'off' signals. Some,[125–128] though not all,[127] previous examples of this rather complex logic array had weak distinguishability between 'on' and 'off' signals.

Layer-by-layer deposition is a useful method to build superstructures from polymers.[129] If these polymers are fluorescent dyes, electronic energy transfer (EET) donor-acceptor systems can be assembled. Kuhn studied conceptually related cases based on Langmuir–Blodgett films in the 1960's.[130] $Zn_2Al(OH)_2$borate units form sheets which have inter-layer galleries which are occupied by various anions.[131] These are layered double hydroxides which are easy to exfoliate as positively-charged nanosheets, on which

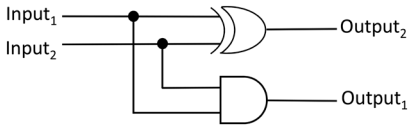

Fig. 4 Physical electronic representation of a half-adder, which is found in the behaviour of **27**.[123]

various anionic species can be adsorbed. Polymers with anionic surfaces such as **28**, **29**-adsorbed double hydroxide nanosheets and **30**-intercalated DNA are blue-, green- and red-emitting inputs, which can be assembled on layered double hydroxide substrates in various combinations for observation by fluorescence.[132] The fluorescence emerges from the energy transfer acceptor.[91] Since the fluorescence output can be observed at the donor or acceptor wavelengths, reconfigurable logic is also demonstrated. An example is a green light output (at 525 nm) is emitted at a 'high' level under 350 nm excitation only if **28** and **29** are present and if **30** is absent. This corresponds to a 3-input INHIBIT logic action (Fig. 6). On the other hand, red light output (at 600 nm) is emitted at a 'high' level only if all three inputs **28**, **29** and **30** are present, which is 3-input AND logic behaviour (Fig. 7).

4. Complex and multivalued logic

This section is longer than it looks. The cases of complex logic within this paper are much more numerous than those present in this section because they fit better under later headings, especially sections 6, 7 and 8. Several, such as 4-to-2 encoders and relatives, have appeared already in section 3. Another 4-to-2 encoder appears in the guise of **31**. Here, the device works on the basis of absorption/emission spectral effects caused by hydrogen bonding or deprotonation due to anion inputs. A much more complex logic system, composed of **32** and **33**, is an edge detector where PET plays a part in the detailed mechanism of action. A short discussion of multi-valued logic in the anion-complexation of **35** and **36** brings up the rear.

If we wish molecules with supramolecular design features to be our intelligent agents, the logic devices discussed up to now can only serve certain functions. Still, these are early examples of SMARTI. However, the availability of more complex molecular logic systems is sure to make our agents more intelligent. Escape from the binary restriction of logic[133] will also add to this intelligence. A selection of recent cases is offered here, while noting that more examples of this type are present within the five applications sections that follow.

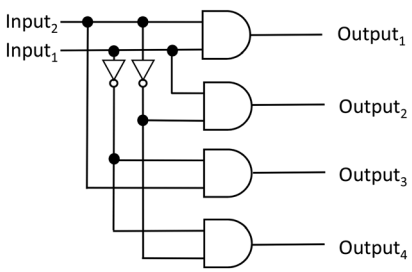

Fig. 5 Physical electronic representation of a 2-to-4 decoder, which is also found in the behaviour of **27**.[123]

Before we examine individual examples, it would be prudent to reiterate the hurdles to more complex molecular logic.[15] A molecular device cannot have identical inputs and outputs because that would cause a short circuit, whereas semiconductor electronic counterparts avoid this problem by providing metal wires as conduits for the input and output signals. Such inputs and outputs would be quantitatively homogeneous. In molecular electronic logic situations, the wiring tends to be much larger than the molecule itself.[134] In most other molecular logic scenarios, conduits are not available anyway and so qualitatively homogeneous inputs and outputs are the best that can be hoped for. This can be achieved with DNA-based devices, inputs and outputs because of the diversity available in rather long oligomers even with only four nucleobases.[135] Such examples will be considered in sections 8 and 9. The approach with a longer history in molecular logic is that of functional integration,[57] where a relatively complicated input–output pattern arising from a rather complicated chemical phenomenon is algebraically analyzed to produce a gate array with NOT, OR and AND units. We note that even some of the 3-input examples discussed in previous sections have benefited from this treatment.

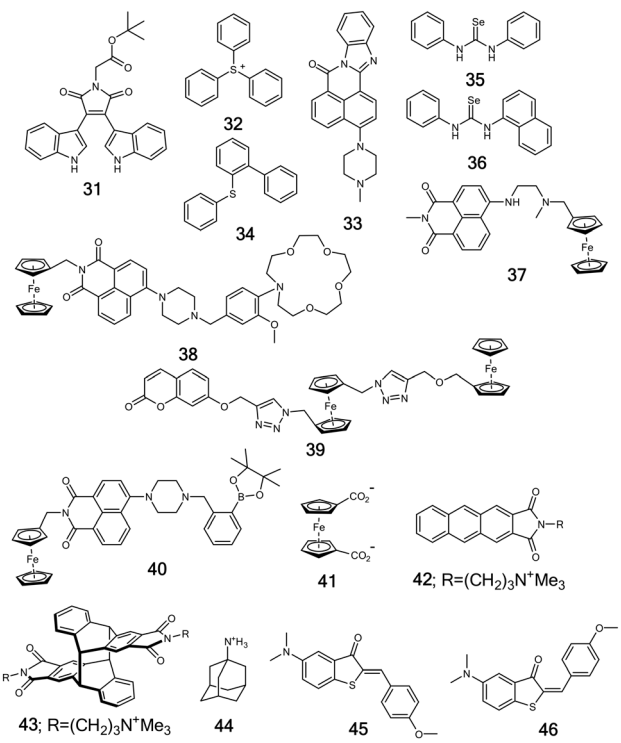

As its name suggests, a 4-to-2 encoder involves four inputs and two outputs (Fig. 8). Such devices are important in computers for binary-to decimal conversions.[15,38] Indeed, the entries in the two output columns of the truth table (Table 1) can be read as '$output_1output_2$' strings to be 00, 01, 10 and

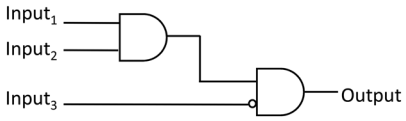

Fig. 6 Physical electronic representation of a 3-input INHIBIT logic gate, which is found in the behaviour of layered double hydroxides involving **28**–**30**.[132]

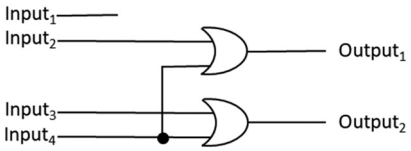

Fig. 8 Physical electronic representation of a 4-to-2 encoder, which is found in the behaviour of **31**.[138]

11 in binary which are 0, 1, 2 and 3 in decimal numbers. Because of their relative complexity, molecular emulators of these are few.[136,137] The anion-dependent optical properties of **31** (ref. 138) can be seen as another case of this type. F^-, CN^-, $H_2PO_4^-$ and I^- are $input_1$, $input_2$, $input_3$ and $input_4$ respectively. $Output_1$ is the fluorescence intensity at 586 nm while $output_2$ is the absorbance at 323 nm. The latter wavelength needs to be carefully chosen so that the corresponding absorbances fit the truth table, though the multi-band nature of absorption spectra (*cf.* emission spectra) aids this choice. It is also critical that THF is the solvent where the anions are able to exert their effects. The fluorescence is quenched by hydrogen bonding or deprotonation of the indole N–H by each anion acting as a hydrogen-bond/Brønsted base with different efficiencies. The same effects control the absorption spectral parameters.

27 (ref. 123) is reincarnated (by the same laboratory[139]) as a 4-to-2 encoder by exploiting its multiple aggregation states. This time, the different states with distinguishable absorption bands are triggered by a series of metal ions applied at rather high concentrations ($\sim 10^{-4}$ M). A type of J (J_b) aggregate, a H aggregate, their mixture or none of them can be arranged with Mg^{2+}, Pb^{2+}, Mn^{2+} and Ag^+ respectively. The '$output_1output_2$' strings in Table 1 can be read as 10, 01, 11 and 00 accordingly. Remarkably, a 7-to-3 encoder arises when a third aggregate (J_a) is added as $output_3$ when three more metal ions (Co^{2+}, Zn^{2+} and Ca^{2+}) are added separately. Even the monomer state of **27** can be brought into play with G-quadruplex forms of DNA (as mentioned previously under the discussion of 2-to-4 decoder in section 3) so that a 14-to-4 encoder becomes possible. This is significant scalability.

Many of the examples featured in this review concern the molecular emulation of a given logic gate array at a time, but now cases are emerging where the molecular function represents rather complex activities of a computer where several logic gate arrays are called into action at different stages of the program or app which is running. These are examples of functional integration of logic gates[57] on a significant scale. Because of their complexity, some of these activities can be found within human behaviour as well. Edge detection is one of these, which is commonly employed to process photographs on telephones and to monitor production lines with machine vision systems[140] – to give just two instances. Remarkably, the same process operates in our eyes all the time when they assess the threat level of an approaching object.[141] The combination of **32** and **33** behaves like these bodyguards in our retinas.[142] Being an industrial photoacid generator,[143] **32** produces H^+ and **34** in response to a dose of 254 nm light. Being a conventional fluorescent PET sensor for H^+, **33** has weak fluorescence at pH 8 on paper but switches 'on' when exposed to photoacid generation at short exposure times. Thus a positive fluorescent image is created when the paper is exposed through a mask. As exposure is prolonged, **34** builds up in concentration to quench the emission of **33** *via* bimolecular PET. "Off–on–off" fluorescence behaviour[144,145] is observed as a result in the exposed regions. At the edges of the exposed regions, however, there is a concentration gradient of H^+ which pushes H^+ to diffuse into the unexposed areas. The moisture level in the paper is controlled so that diffusion of H^+ is restricted to about a millimetre during the experiment. Being far heavier, **34** is essentially stationary during this time. This millimetre of H^+ switches 'on' fluorescence of **33** therein, which becomes the visualized edge. Bacterial cells[146] and reactive DNA networks[147] have performed edge detection previously.

Edge detection happens almost by reflex, and is therefore outside our control. However, the same process underlies an important aspect of human culture which people consciously create. Outline drawing is a part of the visual arts which we all perform but only artists excel in. The outlines which are drawn are the edges of the object(s) as visualized by the artist. Objects of arbitrary curvature and complexity are subjected to the protocol of the previous paragraph[142] so that a positive fluorescent image is created. Subsequent image processing happens as follows. It is expanded by about a

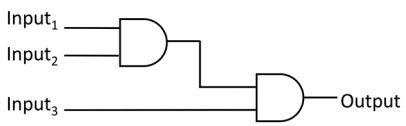

Fig. 7 Physical electronic representation of a 3-input AND logic gate, which is found in the behaviour of layered double hydroxides involving **28**–**30**.[132]

Table 1 Truth table of a 4-to-2 encoder, which is found in the behaviour of **31** (ref. 138)

$Input_1$	$Input_2$	$Input_3$	$Input_4$	$Output_1$	$Output_2$
1	0	0	0	0	0
0	1	0	0	0	1
0	0	1	0	1	0
0	0	0	1	1	1

millimetre, and the original image is quenched or erased to leave behind the fluorescent outline in all its glory (Fig. 9).[148] Quite clearly, molecules such as **32** and **33** can combine to perform the computations involved in an aspect of human culture.

Multi-valued logic naturally carries more information per character than the binary version,[149] but is disadvantaged by its sensitivity to error accumulation within modern computers.[150] The latter occurs because some members of the set '0', '1' and '2', for example, will begin to overlap when the error reaches 50% (which is not unusual after a large number of serial operations) whereas the set '0' and '1' is relatively immune. Molecular logic-based computation, which is currently weak at serial integration anyway, can exploit multi-valued logic by performing low-error operations while preserving the advantage of higher information density. Such a situation arises during the generation of large numbers of molecular identification tags for small objects within substantial populations.[151] While the fluorescence colour and its emission subject to conditions is a basis for molecular logical ID,[152] realistic numbers of tags are produced by combining tags in parallel. Such double tagging (a version of double-labelling) with binary logic gates can produce multi-valued logic gates such as PASS 1 + YES (Table 2).[151–153]

Although the most conveniently observed variables, *e.g.* fluorescence, are the commonest outputs,[30] any phenomenon should be digitizable with the appropriate coding and thresholds. For instance, NMR spectral parameters have been put to use for handling alphanumeric characters.[154] Even host–guest bindings (as inferred from NMR spectra) have been valuable outputs.[97,98] Modes of binding are now employed as outputs with **35** and **36**.[155] These selenoureas capture anions *via* only mono-coordination (coded as 0), mixed mono- and bi-coordination (1) or only bi-coordination (2) depending on the circumstances. Once the inputs are also coded, *i.e.* anions of increasing geometrical complexity, Cl^-, $H_2PO_4^-$, $CH_3CO_2^-$ and $PhCO_2^-$ as 0, 1, 2 and 3 respectively, a multi-valued logic table (Table 3) can be built-up. In contrast to these selenoureas, the corresponding ureas and thioureas are stuck in the well-known bi-coordination mode under most conditions of structure and anion. These observations can be used to add more rows to the logic table, along with an extra column corresponding to chalcogen type – O(0), S(1) and Se(2). Table 3, with/without these enlargements, is another illustration of how chemical interactions can be brought under a conceptual umbrella of computer science.

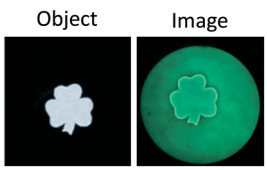

Fig. 9 Outline drawing by edge detection of an object.

5. Redox logic

A series of ferrocene derivatives **37–41** comprises this section where at least one input is an oxidant (Fe^{3+}) or reductant (ascorbate). All of these, except for **41**, work *via* a fluorescence output controlled by PET. **41** is monitored for its current output when it acts as an electron relay between the electrode and glucose oxidase. This makes glucose a natural input. Several logic arrays composed of AND, NOR and INHIBIT gates arise as a consequence.

The mainstream of molecular logic built upon sensors which accepted chemical species such as H^+ as input while releasing fluorescence as output. So it was natural to find many examples of multiple chemical input species driving molecular logic systems.[15] Just as redox indicators[156] appeared alongside the vast bulk of pH indicators in the 20th century,[157] redox-driven cases[158,159] can now be seen as significant contributors to molecular logic research. Like ion-binding equilibria, redox reactions can produce fluorescence switching with similar reversibility so that system reset becomes possible.

37 is interesting because of its 'fluorophore–spacer$_1$–receptor–spacer$_2$–electron donor' format[160] (related to Fig. 3) which allows H^+ and oxidant (Fe^{3+}) inputs. Here, PET is stopped by protonation of the tertiary amine and oxidation of the ferrocene moiety. Green emission from the aminonapthalimide fluorophore is observed in a clear AND logical fashion. Transient absorption spectroscopy offers some evidence in this direction, but no radical ions are unambiguously identified. Interestingly, a system closely related to **37** and carrying a distal benzo-15-crown-5 ether does not confer a Na^+-dependence on the fluorescence output, partly because of the distance of separation and partly because PET to an aminonaphthalimide fluorophore from a benzocrown ether receptor is endergonic.[78] The use of a distal *N*-arylaza-15-crown-5 ether[79] instead reopens this PET channel so that proper three-input AND logic behaviour is seen in the fluorescence output of **38**.[161] The three inputs are H^+, oxidant (Fe^{3+}) and Na^+.

As seen in the previous example **37**, Fe^{3+} oxidizes ferrocene within **39** (ref. 162) in order to stop PET from it to the fluorophore. Ascorbate is the reductant which can reverse the process. This is Fe^{3+}, ascorbate-driven INHIBIT logic since ascorbate inhibits the fluorescence output by re-establishing PET originating in the ferrocene moiety. A closely-related earlier case **40** (ref. 163) is an enabled NOR

Table 2 Logic table of PASS 1 + YES logic[151]

Input	YES output	PASS 1 output	PASS 1 + YES output
0	0	1	1
1	1	1	2

Table 3 Logic table for the different binding modes arising from interactions of **35** and **36** with various anions

Structure	Anion	Binding mode
35	0	2
	1	2
	2	1
	3	1
36	0	2
	1	2
	2	1
	3	0

logic gate where the presence of Fe^{3+} and the absence of ascorbate and F^- produces 'high' fluorescence. Just as in **37**,[160] the ferrocene unit serves as a PET donor to the aminonaphthalimide fluorophore. Oxidation of the ferrocene unit prevents this PET channel. Just as in **39**,[162] the reductant ascorbate recovers the ferrocene state so that fluorescence switches 'off' again. F^- acts more indirectly, by coordinating to the boron centre which appears to retain Fe^{3+} locally so that reasonable concentrations of Fe^{3+} are unavailable to attack the ferrocene unit. Several other enabled NOR gates are known.[164–166]

The use of ferrocene derivatives as electron relays during the electrochemical oxidation of glucose by glucose oxidase is a basis of the diabetes testing industry.[167] Embedding **41** (ref. 168) in a chitin film deposited on a graphite electrode provides opportunities for additional control with H^+ and Cu^{2+} since the latter agents will interact with the amine groups on chitin. Because of the electrocatalytic process, cyclic voltammograms of **41** lose the reduction wave at high glucose levels. Nevertheless, the peak oxidation current is a useful output which shows a positive correlation with concentrations of glucose as well as with H^+. At moderately low pH values, the protonated chitin permits facile diffusion of **41** through the film to carry charge. Thus, an AND gate driven by glucose and H^+ inputs, and giving an oxidation current output is seen. Since Cu^{2+} serves as a reversible inhibitor for glucose oxidase, its introduction as a third input gives rise to a 3-input INHIBIT gate with Cu^{2+} being the disabling input. In keeping with the traditions of semiconductor devices,[38,60] this review divides the analog signals into 'high' and 'low' regions only according to a positive logic convention. This respects the fact that a given device usually has a single convention for coding the signal levels.

6. Information security

Although we have encountered a security application with the edge detection capability of the **32–33** system, it is now time to gather up a bouquet of like-minded cases. Keypad locks or entry codes are represented by **42** and **45**. Both employ light dose as an input while their chemical inputs differ. The outputs of both are the corresponding photochemical products **43** and **46**, one being a photocycloaddition and the other being a double bond photoisomerization. **47** works as a keypad lock by depending on the entire pattern of the absorption spectrum for its output when triggered by d-block metal ion inputs. The security level increases as encrypting messages with **48** is featured. A wide variety of inputs control the pattern of the fluorescence spectrum because of several mechanisms *e.g.* PET, EET and perturbation of ICT excited states. When systems related to **48** are assembled from subsystems, distributed passwords become possible. A way of generating a multitude of encryption keys is illustrated with products, *e.g.* **49**, arising from multi-component reactions. A way of generating a multitude of identification codes for objects is illustrated with the logic types arising from the fluorescence output caused by H^+ input, *e.g.* YES gate **50** which works on the basis of PET.

Meanings of words depend not only on the identity and number of letters but also on the order in which they appear, *e.g.* consider 'tap' when compared with 'cap' (wrong identity), 'ta' (wrong number), 'tape' (wrong number) and 'pat' (wrong order). A telephone number is useful only if the string of decimal digits has the correct length, the correct digits and in the correct order. The same three requirements of identity, number and order, when applied to alphanumeric symbols, appear in the commonest hallmarks of our security conscious society: passwords and entry codes. Naturally, semiconductor-based information technology is well-placed to handle these tasks. It should be equally natural for supramolecular agents to run similar tasks *via* molecular logic. Proof of principle was established in 2007,[169] when the order of application of a set of inputs, not only their nature and number, was demonstrated to be important in eliciting a particular output. Success here requires the device to have a memory. *i.e.* purely combinational logic will not do. Construction of memory from gates requires some degree of logical complexity since history-dependence has to be arranged with feedback, for instance (see later, *e.g.* Fig. 11).

In supramolecular systems, such history-dependence usually translates into the presence of kinetic traps within reaction schemes, although other ingenious approaches have also been applied.[15,170,171] For instance, two molecules of **42** are included within the host cucurbit[8]uril in water and can then be efficiently dimerized because of the enhanced local concentration *via* a [4 + 4] photocycloaddition[172] into **43** with a dose of 365 nm light ($input_1$).[173] When the ideal guest **44** ($input_2$) is added next, **43** is displaced from the host cavity to become free in solution. This is the output (although it is more conveniently measured *via* a fluorescence activation procedure) which is 'high' when 'high' levels of $input_1$ and $input_2$ are applied in that specific order. If the input order were reversed, the first addition of **44** will displace **42** into the bulk water. Without the advantage of high local concentration, the dimerization fails when the UV light dose ($input_1$) is applied next. Then the concentration of **43** in free solution becomes 'low'. A similar 'low' output is obtained when one or both inputs are missing. So the 'high' output

state is found, *i.e.* the keypad lock opens, only for one particular input string.

Although pH-sensitive photochromics have a venerable record in molecular logic research,[67,69,174,175] **45** (ref. 176) distinguishes itself by employing red and green light for its interconversion to/from **46** because of the long-wavelength absorptions of these hemithioindigo derivatives. Keypad lock action is demonstrated by the unique production of **46** as output (above a chosen threshold) upon treatment of **45** with the following three inputs in order: H^+, OH^- and a dose of 505 nm light. This happens because it is only the unprotonated form of **45** which absorbs 505 nm light well enough to produce the *E*-isomer. Any of the other 7 permutations of inputs either leaves protonated **45** which does not absorb the irradiation, or leaves the product **46** in its protonated form which rapidly reverts to protonated **45** at room temperature. Self-annihilating inputs, *e.g.* H^+ and OH^-, have a history in this field.[177]

Most of the supramolecular agents featured in this review rely on electronic emission or absorption spectroscopic outputs because of several advantageous attributes, *e.g.* the ability to communicate with even a single molecule.[178] The single molecule detection capability of fluorescence is particularly well-known since the 1990's.[179–181] This is achieved by taking advantage of the low backgrounds encountered during emission measurements. Modulated absorption can also achieve this.[182] Several logic gates, IMPLICATION,[183] INHIBIT,[183] XOR[184] and YES[185–187] have been explicitly operated under such conditions. The implementation of single molecules as logic devices minimizes the space requirements of a processor and removes ensemble averaging effects.

However, electronic spectra are also characterized by a few broad bands at most which means that they can only convey a limited amount of information. Contrast this to numerous narrow bands present in vibrational spectra, whether infra-red or Raman, which permit valid finger-printing. One ingenious way around this difficulty is the construction of multi-fluorophore systems whose complicated response to analytes provides adequate information density for security application. More about this approach will appear in the next paragraph, but we now discuss **47**.[188,189] Vibrational banding within electronic spectra is not uncommon, but these bands rarely show complicated variation with additives.[190,191] There is a venerable exception however. The Q-bands of porphyrins and their relatives like chlorins[192] vary strongly upon binding metal ions since the pi-systems are perturbed

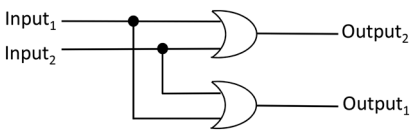

Fig. 10 Physical electronic representation of the logic system underlying the behaviour of **53**.[210]

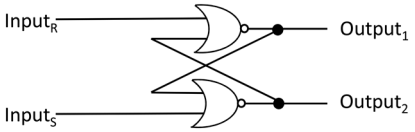

Fig. 11 Physical electronic representation of a RS flip-flop, which is found in a part of the behaviour of **55**/**56**.[219]

directly. **47** is a chlorin whose absorption spectral output responds in this way. The output here is not an absorbance at one specific wavelength but rather the entire spectral pattern which is extracted *via* principal component analysis[193] by considering absorbances at multiple wavelengths. Additionally, metal ion binding to the centre of these pi-systems faces kinetic hurdles in the forward and reverse directions. So, the situation is set for keypad lock behaviour where the four situations – addition of Cu(II) and then Fe(III), Fe(III) and then Cu(II), two doses of Fe(III), or two doses of Cu(II) – produce distinguishable Q-band patterns as outputs. The commercial availability of **47** (as a photodynamic therapeutic[194]) means there is no synthesis investment required either.

The multi-fluorophore, multi-receptor, multi-mechanism system **48** (ref. 195) is a type of combinatorial sensor,[196,197] which possesses a multi-banded fluorescence spectrum with a complicated dependence on a substantial number of analytes. **48** is able to hide a message by combining each of the characters in the string with fluorescence intensity signals arising from a secretly chosen chemical operation which is applied to it. These intensity numbers create the encryption key. This establishes an unpredictably variable code which is, at the same time, reproducible by a recipient who is in on the secret. First, each position on the typewriter QWERTY keyboard is represented by a small range of numbers which has the same order-of-magnitude as the fluorescence intensity. In the coding procedure, each character of the original message will be read in order and allocated a fluorescence intensity number from consecutive specific wavelength intervals in **48**'s spectrum. Then the characters will be coded by adding the average number in the initial small range and the corresponding number from the fluorescence spectrum. This encrypted string of coded characters will be sent to the recipient, who will decrypt it by considering each character and then subtracting the relevant number from the fluorescence spectrum obtained by the same chemical operation performed on the recipient's sample of **48**. Since the output consists of intensities at multiple wavelengths (as mentioned in the discussion of **47**) this entire pattern increases the information density and hence its specificity to a given device structure and its environment. Since only the exact molecular structure of the device and the exact chemical environment will produce the desired output pattern, any adversary would have to reproduce both of these exactly if the secret is to be stolen successfully. Then 'brute-force' efforts to break the code would probably fail. Pre-arranged and carefully controlled

chemical environments, *e.g.* the use of pharmaceuticals or drinks with high quality control because of their human ingestion, are ideal to avoid random interferents which might distort the message.

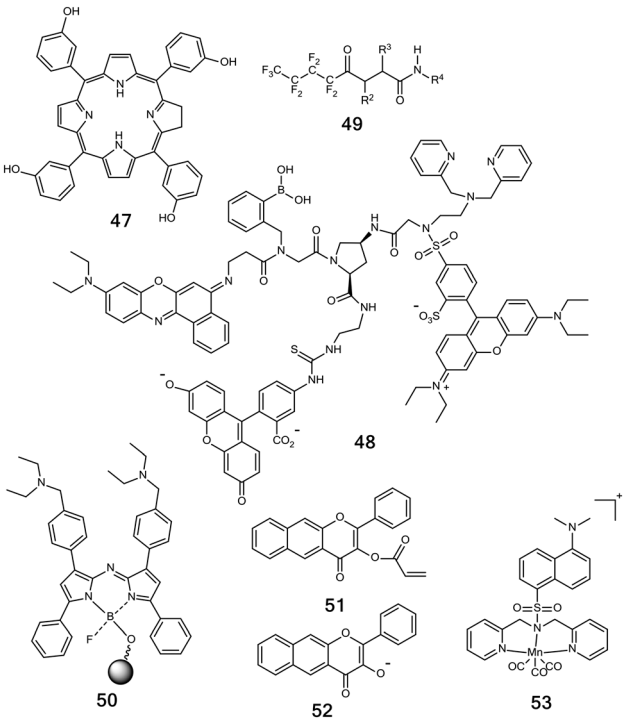

The security of the data transmission is tightened further by applying password protection in the form of keypad locks. Practically usable samples of **48** can also be sent to the recipient by hiding it in a dot within a benign hardcopy message. Supramolecular agent **48** is clearly running an intelligence task here, *i.e.* SMARTI in action.

Some secrets are too big to be entrusted to one person because the consequences of revelation can be devastating, *e.g.* the code to launch a nuclear missile. In such cases, the secret code is divided up among several authorized users. This can be implemented at the molecular level[198] by arranging the self-assembly of an oligomer version of **48** (ref. 195) to result in its attendant benefits discussed above. The multi-fluorophore format is maintained but the platform consists of four DNA strands creating a Holliday junction[199] (where four duplex arms cross) and a G-quadruplex. The latter motif is encouraged to form by sequential addition of Li^+ and Na^+. Each of the strands on the G-quadruplex side terminates in a linker and a fluorophore, with each of these components controlling the degree of electronic energy transfer (EET) between the dyes. Unpredictability of the complicated emission spectral pattern is assured, especially when the response to certain chemical inputs is concerned. The latter is arranged by a degree of the multi-receptor property of **48** being expressed within the assembly by the linkers which are used. Chemometric analysis of the spectral pattern is again necessary to demonstrate the distinguishability of one code from another.

As we saw with **48**,[195] information is secured during communications by applying an encryption key.[200] If this key were a molecule, the common electronic channel could be avoided and it could also be hidden easily among everyday materials in tiny quantities. Once recovered and identified by the intended recipient *via* tandem mass spectrometry, the key will allow the received message to be decrypted. However, such a molecule must be convenient to prepare while containing sufficient diversity. **49** (ref. 201) is such an example of a library which is produced from the Ugi reaction between an aldehyde, an amine, a carboxylic acid and an isocyanide.[202] One of several perfluorocarboxylic acids is chosen in particular, so that the key can be recovered easily by fluorous solid phase extraction.[203] Each of the members of the set of four components will be assigned a code according to their side-chains, from which the encryption key will be built-up.

Identity lies at the heart of many security concerns, and is usually examined with a signature, finger-print, passport or a face. How can this be implemented when the object is microscopic? A fluorescence spectral wavelength maximum is a start,[204] but there aren't sufficient distinguishable numbers because of the broad nature of molecular emission spectra and the limited range of the rainbow. One trick is to make these emissions conditional upon various additives in different logical ways.[152] This topic was touched on in section 4, but the molecular basis is best outlined here. **50** (ref. 151) is a recent case of a YES logic (Fig. 3) tag on a polymer bead where PET from the amines to the fluorophore keeps fluorescence output switched 'off' until a 'high' H^+ input is applied when the emission switches 'on'. If **50** is shorn of its amines, it would become a PASS 1 logic (Fig. 3) tag with essentially the same colour properties but no H^+-induced switching. Such logic tags can confer a degree of distinguishability to a significant population of beads when they are examined with a fluorescence microscope. Related bead-tagging systems carrying components from **37** and **38** produce a variety of logic behaviours driven by H^+ and Fe^{3+}.[205,206]

It is to be noted that several examples featured in this section don't display molecular logic gates explicitly but they are clearly molecular emulations of semiconductor logic-based computations of significant complexity. Therefore, functional integration of logic gates[57] on a noticeable scale is occurring here.

7. Delivery logic

Although the many cases in this review giving fluorescence output can be considered as delivering light, we now concentrate on examples delivering matter. In order of molecular size, CO, **57**, dyes and drugs are delivered. **51** and **53** work on the basis of photodecarbonylation – staples of organic and inorganic photochemistry.[191] These use light dose inputs, along with other chemical inputs such as glutathione, O_2 and H_2O_2. Materials-based gates with

macroscopic valves exploiting gel swelling/contraction or with molecular-scale photodecomposition (*e.g.* **54** with intramolecular hydrogen atom abstraction by excited nitroarenes[191]) will be discussed. Parallel pairs of OR and serial pairs of AND gates are implemented, as well as several other small-scale logic integrations, besides the parent gates themselves. Sequential logic in the form of RS flip-flops are demonstrated with **55**/**56** which deliver **57** as output. The operating mechanism is the geometric fit between host and guest. When **57** serves as input to a downstream INHIBIT gate, fluorescence is the output from **56**. Here, the mechanism is PET.

As the discussion of **1** in section 1 shows, molecular logic-based computation grew out of sensor research and hence the practitioners of the former field have tended to regard sensing as a comfort zone. This has left equally important areas such as delivery of (bio)chemical agents largely untouched by logic concepts, except for a few pioneering cases.[207,208] The following examples begin to rectify this omission.

Benzannelated flavonol acrylate **51** is attacked by thiols to produce the corresponding flavonol.[209] Importantly, these thiols can be intracellular players like glutathione. This is $input_1$. The resulting flavonol **52** fluoresces in green *via* an excited state intramolecular proton transfer (ESIPT) process whereas the starting material emits blue so that they can be optically distinguished. Blue irradiation ($input_2$) of the flavonol in the presence of intracellular dioxygen ($input_3$) creates singlet oxygen as in photodynamic therapy (PDT).[194] Unlike in PDT, in this instance singlet oxygen attacks the very compound that gave it birth. CO extrusion is the output of interest, because of its ability to participate in cell signalling processes. The fluorescence changes are demonstrated intracellularly but apparently not the CO release. Hypoxic cell states, which are important targets in certain disease situations such as solid tumours, do not completely kill CO production as might have been preferred from a diagnostic device with ideal binary logic behaviour. However, the device is useful as is, with appropriate thresholding. The corresponding 3-input AND logic array was encountered previously in section 3 as Fig. 7. The chemical irreversibility of each step is not considered in this logic array due to its single-use application.

53, a tricarbonyl Mn(I) complex with an appended fluorophore, is another logic device[210] with CO as $output_1$ for intracellular signaling application, where $output_2$ is green fluorescence. Interestingly, this device uses violet light as $input_1$ and H_2O_2 as $input_2$. Once excited with light of an absorbable wavelength, Manganese carbonyl complexes decarbonylate. Once all three CO units are shed, all easily fissionable bonds are eliminated causing the fluorescence to be enhanced by an order of magnitude. As in the previous example, only the fluorescence output is observable under intracellular conditions but it serves as a proxy for the CO release. Oxidation of **53** leads to a similar result *via* the collapse of the Mn(II) intermediate. The corresponding logic array is shown in Fig. 10. Co-registering of light and matter in both the inputs and outputs is an interesting feature of this case, as also found with a PDT automaton[211] which will be featured in section 9. Again, **53** involves irreversible phenomena by the very nature of the application.

Implementations of electronic logic gates, *e.g.* diode–diode-logic or transistor–transistor-logic, employed serial and parallel configurations of components.[60] Although not of molecular-scale to allow small-space applications which are barred to semiconductor devices (*e.g.* molecular computational identification),[151–153] molecular-based gel blocks which contract or expand in response to various inputs, *e.g.* pH, temperature, salt, can be combined in various serial and parallel configurations so that they open or close an orifice to switch dye leakage 'on' or 'off'.[212] Although this case concerns dyes, it is possible to imagine extensions to the delivery of various (bio)chemical species in a similar way. We note that these design principles are based on mechanical engineering of valves and not on molecular science, even though the input-responsivity of the gels has a molecular structural design. Such macroscopic logic systems are also available from classical work concerning flow systems,[213] waves[120] or cuvet constellations.[214,215]

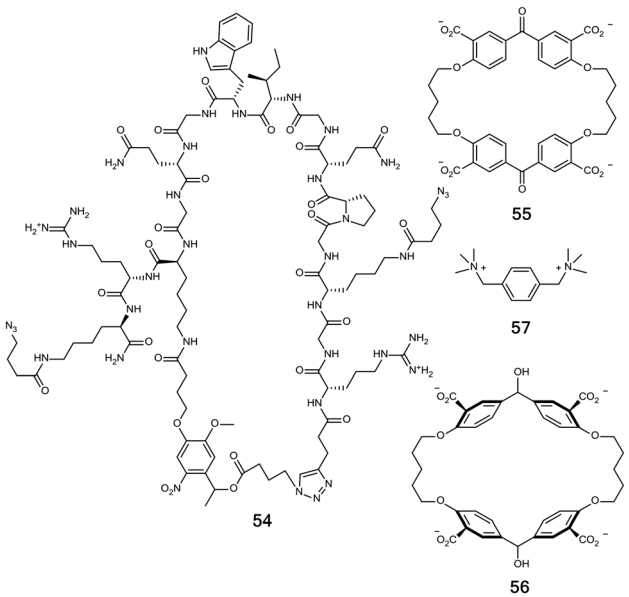

As in the previous case,[212] serial connections give rise to OR logic and parallel connections produce AND logic in cross-linker breakdown to cause hydrogel dissolution so that cross-linked functional molecules or embedded cells are released. YES logic originates from a single connection. However, the present case[216] has all the linkages on the molecular scale. The component connections are a disulfide bond, a specific peptide sequence and a 2-nitrobenzyloxy unit, which are cleaved by a reductant, a collagenase and UV light respectively. Although the 2-nitrobenzyloxy group and the disulfide reducibility are classics in photochemistry[172] and biochemistry[217] respectively, and the collagenase specific

peptide sequence is from the 90's,[218] these have been logically combined in the present application. An example cross-linker **54** (ref. 216) contains the special peptide sequence at the top and the photosensitive group at the bottom whereas the two azide units on the sides permit click-type connections to the drug and to the rest of the substrate so that the drug is released in a light, collagenase-driven AND logical fashion.

Combinational logic devices require their outputs to respond quickly without hysteresis to the status of inputs presented to them. In their molecular incarnation, this means that weak interactions, which can be made and broken rapidly, need to be employed so that the device can switch between the various states/configurations over a short timescale. Supramolecular interactions, provided that they are not grouped together in too large a number, would fit the bill owing to their dynamic chemical reversibility. On the other hand, sequential logic or memory devices require their outputs to latch in a given state irrespective of the input status until a specific input command is received.[38] Furthermore, toggling of the output needs to be arranged. Molecule-based sequential logic therefore can be based on strong bonds which are stable over time until the appropriate chemical reactant is applied. Classical molecular chemistry, which is built on specific bond-making or bond-breaking reactions, is ideal for this purpose, especially if the toggling requirement is waived for single-use applications. Unlike in electronic computing, there are many situations in (bio)chemical contexts where this waiver is tolerable. When toggling of the output state is essential, interconverting pairs of chemical reactions are available, *e.g.* reduction of ketones and oxidation of secondary alcohols. Of course, classical (bio)chemical reactions can also be used to produce single-use combinational logic devices when history-dependent effects are not being considered. A key advantage of supramolecular interactions is that the structural identity of the logic device is conserved. Interconverting pairs of chemical reactions are also well-behaved in this regard since the two-structure system can be identified as the device.

We used these general considerations to design the specific case **55**/**56**.[219] When dissolved in alkaline water, dialcohol **56** contains a reasonably deep hydrophobic cavity which has the appropriate size, shape and nature[220] to inclusively bind the dicationic guest **57**. On the other hand, diketone **55** has collapsed phenylene walls owing to their pi-delocalization with the carbonyls and is therefore unable to hold this guest. This is molecular-scale delivery. Such a guest capture-release system can now be understood as a molecular memory, since either of these two redox states is stable towards more or none of the reagent which gave it birth (say, the reductant which created dialcohol **56**). Only the opposite interconverting reagent (*e.g.* oxidant) causes it to flip to the other state (*e.g.* **55**). Either of the two states of the fundamental computer memory, the RS flip-flop,[38] has the same stability towards application of the same input which created it (*e.g.* set input) or the application of no input at all. A given state of the RS flip-flop can be flipped by application of the opposite (*e.g.* reset) input. The corresponding logic array (Fig. 11) and the truth table (Table 4) are shown.

The **55**/**56** contains an additional feature of self-indicating its state of guest occupancy, which produces a more integrated gate array (Fig. 12). When guest **57** is bound within the host **56**, PET can be seen to occur from the oxyphenylene units of the host to the electron deficient phenylene unit of the guest upon application of a version of eqn (1). The host **56** is therefore fluorescent in the absence of a guest but switches 'off' upon binding **57**. Thus, downstream INHIBIT logic processing of memory-based delivery is seen.

It is clear that delivery of various (bio)molecular agents according to algorithms defined by the scientist will provide useful solutions to problems at the molecular- and materials-levels.

8. DNA and protein logic

A clear success of molecular logic-based computation is that large numbers of bioscientists have felt persuaded to join the field with their biomolecules and biomolecular systems (Fig. 1 and Table S1†). SMARTI is evidently prospering even more in the biosciences than in the chemical sciences. Compounds **58**–**80** will be discussed here. The supramolecular agency is seen in the hydrogen bonding interactions driving the pairing of nucleobases. In much of DNA computation, the original combinatorics path[221] has now been essentially abandoned[222,223] in favour of the logic road.[224] Still, many bioscientists remain blissfully unaware of the chemical beginnings[14,57,77] of their research, even though the early adherents[225–228] acknowledged the origin.

Beside straightforward strand hybridization, certain secondary structures are crucial for device design. The first half of this section concerns devices exploiting stem-loops, G-quadruplexes and i-motifs. The first of these revolves around its ability to catalyze the decomposition of a target DNA strand (**58**–**64**) and an example of a 1 : 2 demultiplexer is detailed. G-quadruplex systems **65**, **67**, **70**–**73** and **74**–**78** give rise to logic types as simple as PASS 1 and as complex as 4-to-2 encoders and 2-bit parity generators. However, simplicity is no disrespect here because the ideas behind PASS 1 can be developed into graphical displays (see later). An acid-triggered i-motif features in **79** during the demonstration of a NAND gate. The second half of this section concerns devices

Table 4 Truth table of a RS flip-flop, which is found in a part of the behaviour of **55**/**56** (ref. 219)

$Input_R$	$Input_S$	$Output_1$	$Output_2$
0	0	Holds previous state	Holds previous state
0	1	1	0
1	0	0	1

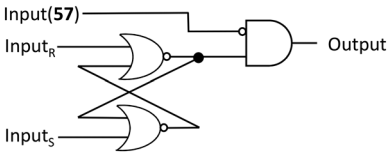

Fig. 12 Physical electronic representation of the logic system underlying the behaviour of **55**/**56**.[219]

working on the basis of toehold-mediated strand displacement. Improvements such as fuel strands and thresholding strands will be discussed. Such devices allow cascading of several gates in series. Another improvement to be considered is strand displacement which can be accelerated when mediated by a DNA polymerase. The principle of building gates out of switches in series or parallel[60] is also applicable to DNA and is considered next. Almost all of these examples depend on fluorescence as the output, usually from covalently attached fluorophores but coordinatively or supramolecularly associated emitters (*e.g.* **66**) are also employed. In many cases, the emission is switched 'on' by disconnecting a quencher from the emitter so that EET between them ceases. Occasionally, *e.g.* in **65**, the distance-dependence of PET is also exploited. Rarely, absorption serves as the output, *e.g.* the oxidation product of **69**. Since a recent book collects the large literature on enzyme logic,[20] this section concludes with a footnote in terms of a couple of gates concerned with enzymes alone.

DNA-based enzymes or deoxyribozymes have a played a key role in the development of molecular logic[229] by operating on a substrate strand carrying a single ribonucleotide as its weakest point and a fluorophore-quencher pair at its termini. Hydrolysis at the weak point separates the quencher from the fluorophore so that the emission output is switched 'on'. Extra diversity has been built into such systems by constructing catalytic stem-loops out of three or four subunits.[230,231] For instance, a 1 : 2 demultiplexer (Fig. 13) is assembled as follows. When the address input is '0' the data input goes to output$_1$ or if the address input is '1' the data input goes to output$_2$, requiring AND and INHIBIT logic devices. **58** and **59** combine with input$_{Data}$ (**60**) to form the stem-loop construct, which hybridizes with a substrate (**61**) in order to hydrolyze it and liberate fluorescence from fluorophore$_1$. This is output$_1$ 'high'. Naturally, this process would not happen if input$_{Data}$ (**60**) is absent (Fig. 14a). This overall situation applies when input$_{Address}$ (**62**) is absent, indicating

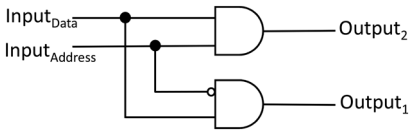

Fig. 13 Physical electronic representation of a 1 : 2 demultiplexer, which is found in the behaviour of **58**, **59**, **61**, **63** and **64**.[230,231]

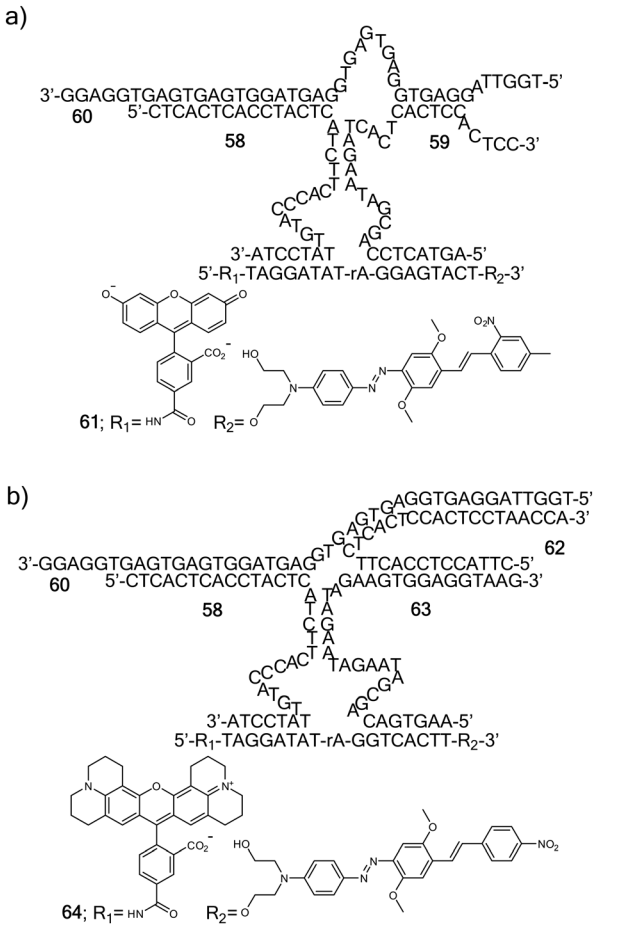

Fig. 14 Sets of DNA strands (a) **58**–**61** and (b) **58**, **60**, **62**–**64** in their hybridization configurations.

INHIBIT logic behaviour of the device composed of **58**, **59** and **61** strands. If **62** is present, a more stable stem-loop construct is produced with additional components **58** and **63**, along with input$_{Data}$ (**60**). Now the chosen substrate is **64**, which hydrolyzes to liberate fluorescence from fluorophore$_2$ so that output$_2$ goes 'high'. Naturally again, this process would collapse if input$_{Data}$ or input$_{Address}$ are absent (Fig. 14b), indicating AND logic of the device composed of **58**, **63** and **64**. This completes the contents of the truth table (Table 5).

DNA logic without catalysis is illustrated by **65** (ref. 232) has a cytosine-rich run which allows for hairpin formation *via* cytosine–Ag$^+$–cytosine linkages. It also has a guanine-rich run which allows for G-quadruplex formation organized

Table 5 Truth table of a 1 : 2 demultiplexer, which is found in the behaviour of **58**, **59**, **61**, **63** and **64** (ref. 230 and 231)

Input$_{Address}$	Input$_{Data}$	Output$_1$	Output$_2$
0	0	0	0
0	1	1	0
1	0	0	0
1	1	0	1

around Pb^{2+}. When **65** is folded up in this way, the electron-poor hexachlorofluorescein terminal is brought close to the electron-rich guanine set so that a PET process occurs to switch 'off' the fluorescence output at 556 nm. The enforced proximity of the heavy atom Pb^{2+} to the fluorophore may also play a role in this quenching.[191] Thus, the fluorescence output responds to the two inputs, Ag^{+} and Pb^{2+}, in a NAND logical (Fig. 3) fashion.

As discussed in section 4, a 4-to-2 encoder (Fig. 8 and Table 1) reads $input_1$, $input_2$, $input_3$ and $input_4$ in order to produce the output string '$output_1output_2$'. $Output_1$ is the 617 nm emission of an Ag nanocluster bound to cytosine-rich runs of an oligonucleotide,[233] while $output_2$ is the 620 nm emission of *N*-methylated porphyrin **66** which seeks out G-quadruplexes. The closeness of the wavelengths would mean these outputs will need to be measured in separate experiments. 35-mer **67** is the device, which is label-free but possesses a receptor for the Ag nanocluster. $Input_1$ is a 17-mer which hybridizes with **67** but the duplex has no cytosine-rich or guanine-rich runs to trigger nanocluster or **66** emission respectively. So we have a '00' output string as its response. Notably, nanocluster emission switches 'on' when it is held within the duplex region, perhaps by protection from the solvent water. $Input_2$ is a 29-mer which is nicely complementary to **67** and possesses a cytosine-rich run in addition to the sequence of $input_1$. So the Ag nanocluster emission alone is switched 'on' to create the output string '10'. $Input_3$ is a 35-mer built-up from $input_1$ which is not only complementary to **67** but produces a G-quadruplex in the process of hybridization. So the output string is '10' this time. $Input_4$, being a 53-mer carrying most of the sequences of $input_2$ and $input_3$, gives rise to the output string '11' upon hybridization with **67** to complete the 4-to-2 encoder truth table.

Medical doctors diagnose disease states of patients from laboratory test data according specific algorithms. Molecular logic systems inspired by such situations[58,228,234] can give a single 'off'/'on' readout to enable a 'well/ill' decision. If molecules displaying different logic types are placed in a well-array, signal patterns can be produced.[235] Alphanumeric characters would be a particularly communicative signal pattern[236] to convey the 'well/ill' decision. This idea is developed with a 3 × 5 well-array being chosen to display 'O', 'P' or 'F' to signify 'no illness (tuberculosis)', 'ill but treatable' or 'ill but drug-resistant' respectively.[237] As discussed in the previous paragraph, G-quadruplexes bind to porphyrin derivatives. If the latter is hemin (**68**), we have an peroxidase catalyst assembly to convert **69** into a green coloured product. Thus, guanine-rich **70** generates a green output signal in a PASS 1 (Fig. 3) manner, *i.e.* irrespective of the inputs applied. The corresponding PASS 0 gate is represented by aqueous buffer lacking any oligomer so that a catalyst assembly is precluded. The corresponding YES gate (Fig. 3) is constructed by assembling two halves of **70** (minus the central cytosine) when an input strand **71** mimicking the drug-susceptible bacterial DNA is applied. Only then does the oxidation catalyst assembly kick in. The device in this case consists of two stem-loops **72** and **73** which open upon hybridization with the input strand to expose the assembled G-quadruplex. Several other gates are constructed according to similar principles to complete the task being run.

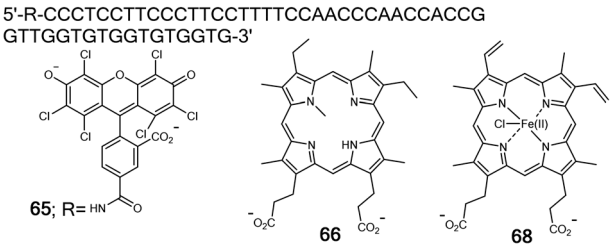

5'-R-CCCTCCTTCCCTTCCTTTTCCAACCCAACCACCG
GTTGGTGTGGTGTGGTG-3'

5'-CCCTAACTCCCCAGCACATCTGATAGTTCTATGCT-3'
67

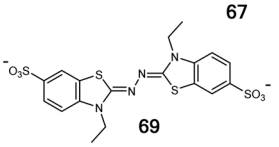

5'-GGGTAGGGCGGGTTGGG-3'
70

5'-GGACCAGAACAACCCGCTGTCGGGGTTGACCCACAAGCGCCG-3'
71

5'-GGGTTGGG-triethylene glycol linker-AACCCCAACAGCGGGTTGT-3'
72

5'-CCCTATGTGGGTC-triethylene glycol linker-GGGTAGGG-3'
73

5'-ATACAGTAATAGGGGTGGGATAAGAAAGTACAA-3'
74

5'-TTGTACTTTCTTATGGGTGGGT-3'
75

5'-TGGGTGGGCTATTACTGTAT-3'
77

5'-ATACAGTAATAGCCCA-3
76

5'-ACCCATAAGAAAGTACAA-3'
78

Although we are introduced to odd/even numbers in childhood, it is notable that information technology uses parity for determining fidelity of data transmission by adding a parity bit to data strings.[38] Molecular versions of parity checkers and generators were first constructed with photochromics.[238] These are based on XOR logic, since its output when added to its inputs always gives even parity (Table 6). So, a 2-bit data string when combined with a check bit generated by applying XOR logic to the data bits will maintain even parity if there is no corruption during transmission. Any change of the total parity to odd would indicate a bit has been flipped by corruption.

A DNA-based version of the parity generator is illustrated with **74** (ref. 239) which contains half a G-quadruplex as its mid-section. If the other half is provided by a suitable input, the resulting hybrid can bind **66** (ref. 231) to produce a 'high' fluorescence output at 620 nm. Each data bit is made up by a mixture of two oligomers: $input_1$ is **75** and **76**. $Input_2$ is **77** and **78**. It is notable that the components of $input_1$ and $input_2$ annihilate each other pairwise because long stretches of them are complementary to each other. Such self-annihilation of inputs is a tested approach to constructing XOR logic gates.[177]

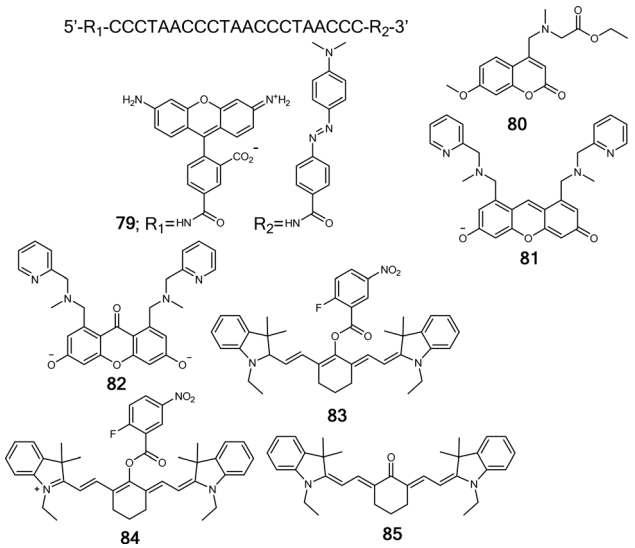

Like the G-quadruplex which starred in the previous paragraphs, the i-motif is another quadruplex structure which has been exploited in logic devices, one of which was discussed in section 3.[123] As mentioned there, cytosine-rich runs give rise to this structure in acidic solution. So, a DNA strand carrying an energy donor–acceptor pair at its termini can be folded into the i-motif to switch 'off' emission of the donor. Uniquely, the necessary acidification for **79** is provided by enzyme inputs.[240] The venerable examples of invertase being required to break sucrose down to glucose and glucose oxidase being needed to produce gluconic acid set up the requirements for NAND logic (Fig. 3) behaviour in the emission of **79** driven by invertase and glucose oxidase inputs.

A scalable approach to DNA logic without catalysis[135] exploits qualitative homogeneity of inputs and outputs (as mentioned in section 4). This uses strand displacement which is aided kinetically by the presence of overhangs or toeholds in a duplex,[241] so that the product of a given reaction step is available to engage in a subsequent step. AND gates are the most straightforward to achieve in this way (Fig. 15a). The device can be viewed as a duplex with a nick or as a hybrid composed of three strands. Importantly, the device has a toehold which allows it to interact with $input_1$. In effect, $input_1$ strips off one of the strands to expose another toehold. This second toehold is then exploited by $input_2$ to dismantle the original device further. Such dismantling can separate a quencher from a fluorophore to produce a 'high' emission output. This final step where a chemical input produces a light output, *i.e.* heterogenous input and output, is necessary for interfacing molecular devices with human operators since its use in the very first molecular logic gate.[14] OR gates upstream of AND gates can also be implemented with aid of translator gates (Fig. 15b), so that identical strands become available from both inputs for presentation to subsequent AND gates. Although XOR logic implementation remains difficult,[242] Fig. 16 illustrates the level of logical complexity achievable in this way. The fidelity of such devices has been improved recently.[243]

The method of the previous paragraph has finite scalability in terms of serial integration since input strands get used up by sequestration during strand displacement and so lose the potency to drive the displacement equilibrium by mass action. This situation can be improved by providing a fuel strand to release input strands from their sequestered versions by a separate displacement (Fig. 17a).[244,245] Note how the toehold on the gate which is used for the fuel, input and output alternates between the twins which are available. The idea of fuelling DNA logic gates harks back to the power supply present in the first molecular logic gates[14] and in conventional semiconductor gates[38,60] as well. The fuel strand stays inactive when an input strand is absent. Another improvement is the provision of a threshold device which contains a longer toehold than usual so that it reacts faster with the input strand than the gate-output complex (Fig. 17b). It is only once the threshold is used up that the remaining input strands can attack the gate-output complex. This example can be converted to a YES gate with fluorescence readout by using a reporter containing a fluorophore-quencher assembly which is disassembled by the output strand.

If two inputs with identical toeholds and recognition regions are considered at equimolar concentrations, a first gate-output complex (without assisting fuel or threshold) is employed to effectively sum the concentrations of the two inputs. This is then fed to a second gate-output complex of the type discussed in the previous paragraph. Now, the use of a small (sub-equivalent) concentration of threshold device would mean that it would be overwhelmed even when either of the original inputs are present alone. Thus, the gate-output complex would be attacked to finally release 'high' fluorescence. This would be OR logic action. On the other hand, if a slightly higher than equivalent concentration of the threshold device is employed, both inputs need to be added before the any input strand becomes available to the gate-output complex. Thus, AND logic is attained. Gate arrays as complicated as the one calculating integer square roots of a four-bit number (Fig. 18) are demonstrated according to this protocol.[245]

According to electronics textbooks,[60] two (or more) switches can be wired in parallel or in series to produce OR or AND logic gates, respectively. Molecular implementations of this should be possible in the near future for the case of electronic conduction output of photochromic units under various stimulations.[101,102,246] Section 7 mentioned related

Table 6 XOR logic truth table and summed parity for each row, demonstrating a 2-bit even parity generator, which is found in the behaviour of **74** (ref. 239)

$Input_1$	$Input_2$	Output	$\sum$parity
0	0	0	Even
0	1	1	Even
1	0	1	Even
1	1	0	Even

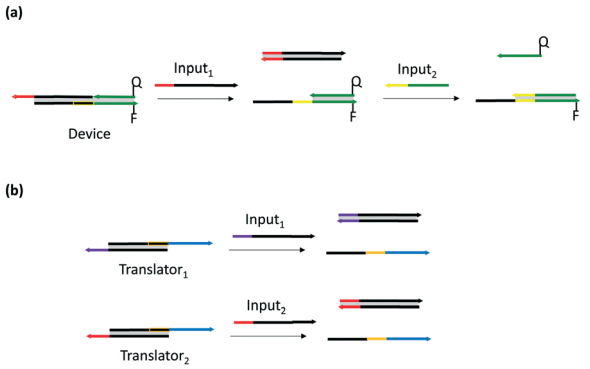

Fig. 15 (a) Two-input AND logic gate[135] using toehold-mediated strand displacement. Complementary runs are shown in identical colours. Hybridized regions are shown in grey. F = fluorophore and Q = quencher (matched with F for efficient quenching *via* EET). The shortest runs are toeholds or, when highlighted with a rectangle, hidden toeholds. (b) The use of translator gates to effect a two-input OR gate for feeding a downstream AND gate.

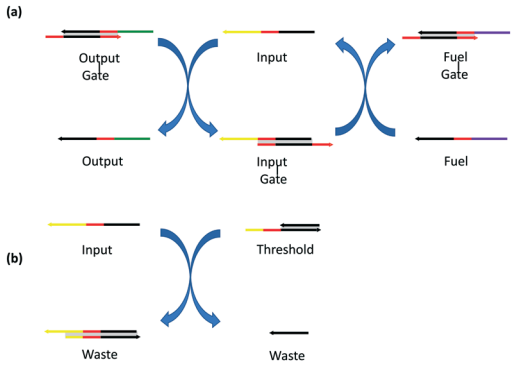

Fig. 17 (a) The use of a fuel strand to regenerate an input strand to drive output strand formation. (b) The use of a threshold device. Complementary runs are shown in identical colours.

cases concerning valves based on gel swelling.[212] This fundamental idea is now realized with DNA devices[247] based on toehold-mediated strand exchange.[135] Fig. 19a shows the basic version of a two-input AND gate. Clearly, this is a 'switch$_1$–connector–switch$_2$' system, where both switches must be flipped 'on' for the output conductance to be 'high'. Of course, the connector needs to conduct as well. In the DNA scenario, this last point is crucial. Fig. 19b details how this is achieved. Switch$_1$ is initially 'off', as indicated by the unhybridized nucleotides. More importantly, it has two overhangs, one of which is exploited by the input$_1$ strand as a toehold to strip off a strand from switch$_1$. The fully hybridized version of switch$_1$ (the 'on' state) is now formed. The value of this switching 'on' is really in the production of a new single strand, which becomes the 'current signal$_1$' in the sense that it is where the action is now. The 'current signal$_1$' strand approaches another gate component which contains a receptor site for it *via* a suitable toehold. This gate component also contains a receptor for input$_2$ which is presently hidden but becomes available once 'current signal$_1$' strand does its stripping job. It is notable that the product from switch$_1$ becomes the starting material for switch$_2$ which serially couples switch$_1$ and switch$_2$. Somewhat similar serial gate integration was seen in **56** acting as a receptor for **57**.[219] The end result is the production of 'current signal$_2$' because switch$_1$ and switch$_2$ are now both 'on'. This end result is visualized as a fluorescence output by using a reporter containing a fluorophore–quencher assembly which is disassembled by the action of 'current signal$_2$'. Similar concepts, though with different implementation, were reported in 2011.[244]

OR gates are built in a similar way but with parallel switches and NOT gates are arranged by building-in receptors for the complement of the relevant input strands. Another positive feature of this work is the reduction of timescales from the usual hours[135] to minutes. This method also permits calculation of integer square roots[245] (Fig. 18), only faster.

Similar increases of speed are realized with polymerase-mediated (rather than toehold-mediated) strand displacement on double[248]- or single-stranded[249] gates. The levels of gate integration are not dissimilar either. Once it is primed, the polymerase keeps adding the appropriate nucleobases to the primer and displaces the old strand.

In a giant undertaking, the square root calculator has been extended to 10 bits[250] using toehold-mediated strand exchange.[135] In closing this section, it is worth noting that cases of this type only permit 'single-use' computations without sequential logic components.

An example of an enzyme input (a robust lipase) being combined with an atomic input (H^+) is provided by **80**.[251] A 'fluorophore–spacer$_1$–receptor–spacer$_2$–enzyme substrate' (related to Fig. 3) system is present here, where the 'fluorophore–spacer–receptor' system of say, **5**,[2] is extended to accommodate an enzyme responsivity. Once the lipase hydrolyzes the ester, the resulting carboxylate moiety is significantly less electron-withdrawing. This shifts the pK_a

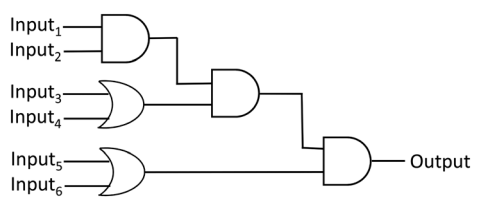

Fig. 16 Logic array achieved in ref. 135.

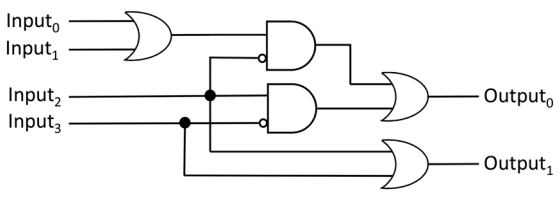

Fig. 18 Minimized logic gate array representing the calculation of '(input$_3$input$_2$input$_1$input$_0$)$^{1/2}$'to give the result 'output$_1$output$_0$'.

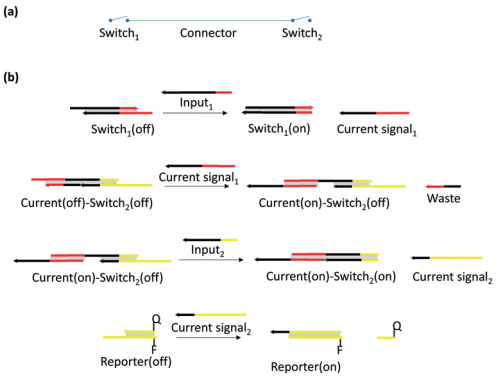

Fig. 19 (a) Serial switches for a two-input AND gate. (b) Molecular implementation with toehold-mediated strand exchange.[247] Complementary runs are shown in identical colours. Hybridized regions are shown in grey. F = fluorophore and Q = quencher (matched with F for efficient quenching *via* EET). Hidden toeholds are not shown explicitly.

value upward from 3.6 to 6.7, so that the fluorescence at pH 6 switches 'on'. No such switching 'on' is seen at pH 10, as expected from lipase, H^+-driven AND logic.

In contrast to the case in the previous paragraph, the bulk of the examples of logic concerning enzymes[17,20,23,252] concerns oxidoreductases. Chimeric versions of these can deliver even more complex logic operations. For instance, glucose dehydrogenase can be fused with calmodulin[253] so that the glucose oxidation depends on the calmodulin existing in a folded form. The latter process requires the presence of Ca^{2+} ($input_1$) and a myosin-based calmodulin-binding peptide ($input_2$). When glucose ($input_3$) is added, a suitable dye can be reduced. When the latter is taken as the output, 3-input AND logic (seen previously in Fig. 7) is found.[254] An electron mediator is also necessary to enable the oxidation/reduction and could be considered as a fourth input in a 4-input AND device.

The expansion of intelligent supramolecular agents to include polynucleotides since 2003 (ref. 226) and the availability of an extensive body of work on polyaminoacids achieving related goals[20] give SMARTI a much broader platform than before.

9. Intracellular logic

The early hype surrounding molecular logic was that computers could be shrunk[255] but this ignored the difficulty of serially integrating practical gates of this type. From its inception as an experimental science,[14] it was realized that the strong suit of molecular logic-based computation was its ability to operate in small and biocompatible spaces. A micrometric cell is a far less confined space to a molecule than it might seem to us. Although the first demonstrator was a simple soap micelle,[256] substantial numbers of examples are now emerging where the spaces inside living cells are becoming molecular logicians' playgrounds.[257–259] The conceptual jump from bulk solution in a cuvet to an intracellular environment was made possible by prior successes in intracellular sensing,[260] where issues of variable optical pathlength, variable device concentration and variable quencher concentrations were dealt with when necessary. Problems of arranging entry into the cell and of preventing expulsion or destruction were also solved to some extent. These earliest intracellular sensors are now understood to be YES or NOT logic gates or their superpositions.[25] More complex logic gates operate within a similar conceptual framework. Placing logic gates within cells allows monitoring of various chemical input concentrations as the cells live their lives. The following discussion is a snapshot of this vibrant direction where supramolecular agents are clearly running tasks intelligently on our behalf in these tiny and vital spaces. SMARTI has this unique stage to shine on.

In the intracellular domain, AND logic has tended to be particularly dominant so far. This is a natural development in terms of complexity after the success of single-input gates such as YES and NOT in this new milieu. Also, there are many examples of the coincidence of species which cause vital cell processes which represent AND logic anyway. So, a burgeoning of fluorescent AND gates to visualize these situations is to be expected. **81**, **83**, **86**, **92–95** and **99** are some of these. These are performing non-trivial tasks. Many of these work on the basis of fluorescence-PET competition, although some operate *via* the chemical transformation of a fluorophore, *e.g.* **81**, **86** and **92**. However, further logical complexity is also expected to emerge. With the aid of fluorescent intermediates **87–89**, **86** also displays 2-to-4 decoder action. A 1 : 2 demultiplexer is demonstrated with **100**, where fluorescent and photodynamic therapy outputs are switched. Other integrated logic arrays arise from DNA and RNA devices, as well as engineered yeast systems. Some of these produce their fluorescent output by activation of a gene for green fluorescent protein, while another relies on EET between fluorophore–quencher pairs. These and their mechanism of operation will be discussed below.

81 is an early example of a logic gate operating within autolysosomes to signal the co-occurrence of H^+ and H_2O_2.[261] Autolysosomes need such extreme conditions to recycle mitochondrial components. The oxidation at the meso-position requires the two pyridylmethylamino units lining the cleft and also requires pH values at the acidic end of the physiological range. The product **82** emits at a shorter wavelength (450 nm, excited at 380 nm) than **81** (520 nm, excited at 480 nm) and this permits ratiometric monitoring for purposes of reliable quantitation. In both cases, protonation of the amine groups suppress PET from them to the fluorophores.[2] Observation of output at 450 nm corresponds to AND logic whereas monitoring at 520 nm gives NAND logic action (see Fig. 3). Such wavelength-based reconfiguring of logic[15] could have been discussed in section 3. Co-localization studies show that **81** goes to mitochondria and that **82** goes to lysosomes, from which the autolysosomes are produced.

83 (ref. 262) is particularly interesting because it targets, albeit irreversibly, two species which can annihilate each

other but which are nevertheless produced in mitochondria for redox balancing – H_2S_n and $O_2^{\bullet-}$. Since **83** is a reduced cyanine dye, this hydrocyanine can be oxidized by $O_2^{\bullet-}$ to the more pi-conjugated cyanine form **84** which emits weakly at 794 nm since the PET-type acceptor (the fluoronitrobenzoate unit) is present. The latter can be ejected from the main skeleton of **83** by the conjugate base of H_2S_n due to the nucleophilic aromatic displacement of fluoride followed by intramolecular attack on the carboxylate unit to complete the ester hydrolysis. Then the product **85** emits 18-fold stronger, but at the shorter wavelength of 625 nm owing to it being a cross-conjugated ketocyanine. The mitochondrial location of **83** and its products is demonstrated by co-localization experiments in macrophage cells. Due to the deep tissue penetration of red and near-infrared emissions of **84** and **85**, even live mice can be studied after intraperitoneal injection of **83**. Phorbol 12-myristate 13-acetate and lipopolysaccharide are employed to trigger $O_2^{\bullet-}$ and H_2S production respectively. However, lipopolysaccharide is also known to stimulate production of reactive oxygen species in macrophages[263] which complicates interpretation of the last results. However, the overall AND logic behaviour of **83** driven by H_2S_n and $O_2^{\bullet-}$ inputs while delivering an output of fluorescence at 625 nm is not in doubt.

Since the bulk of examples in this section target small molecular species, being able to target two enzymes as inputs takes intracellular logic gates in new biomolecular directions.[257,259] When exposed to an esterase and a phosphatase, **86** gives rise to a fluorescence output at 536 nm from the product **89** in an AND logical fashion.[264] The phosphatase alone produces **87** emitting at 558 nm, while the esterase alone produces **88** emitting at 448 nm. On its own, **86** fluoresces at 472 nm. All four emissions are visually distinguishable. Impressively, all four species emit maximally with near-unity quantum yields under physiologically accessible pH values. Under these conditions all carboxylic acids and phosphoric acids are ionized, and even the phenols are ionized in their excited states during fluorimetric observation.[90] Hence, **86–89** are all shown in their ionized states. Then it is possible to understand the order of their emission wavelengths according to the electron-push or -pull ability of each substituent within the ICT state.[91] Once internalized in fibroblasts, phosphatase activity is seen, followed by a slower esterase activity. Simultaneous excitation at two wavelengths (395 and 460 nm) permits excitation of all four species so that intensity responses at four carefully chosen wavelengths (436, 498, 528 and 576 nm) produces the action of a 2-to-4 decoder. This logic type was discussed previously in section 3 (Fig. 5). Here, a 'high' signal is outputted in only one of the four channels for each enzymatic input condition. In other words, data bits arriving in two channels are decompressed into four channels.

The classical fluorophore fluorescein **90** contains two potential phenol units which can separately carry two orthogonal protecting groups R_1 and R_2. Then it would require the presence of two separate input species to deprotect the two phenols so that the push–pull[91] phenolate–quinone **29** would be revealed at near physiological conditions. Such AND logic behaviour is spoiled somewhat by the moderate fluorescence seen in the monoprotected intermediates. The latter problem disappears when the ether oxygen is mutated into a sp^3 hybridized carbon to give **91**.[265] This is orthogonally protected by a mono-β-galactoside and a mononitrobenzyl unit to give **92**. Now, both β-galactosidase enzyme and 365 nm light dose are necessary for fluorescence to flare up at 567 nm. **92** contains a pentafluoroaryl sidechain for reaction with intracellular glutathione for retention inside fibroblast-like cells with enhanced β-galactosidase levels. Now the AND logic action results in a fluorescence intensity enhancement factor of ~10.

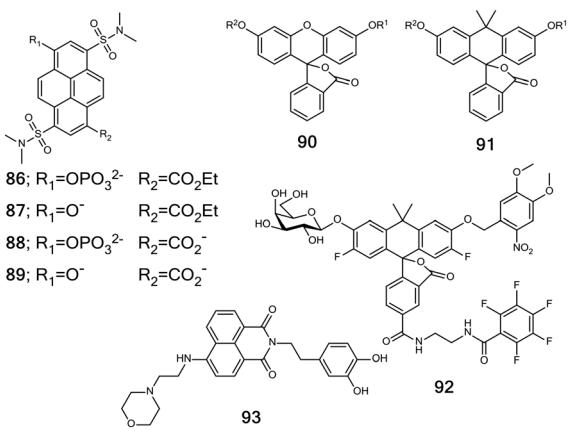

Another example of signaling the co-occurrence of H^+ and H_2O_2 is **93**.[266] The aminonaphthalimide with an aminoethyl sidechain is a well-recognized PET system for fluorescence switching 'on' in the presence of H^+.[267] Such a motif is also common within compounds which locate within acidic lysosome compartments.[268] Electron-rich phenols have been employed as electron donors within luminescent PET systems,[269] and so the catechol unit should be able to launch a PET process across the dimethylene spacer if the thermodynamics are suitable. Therefore, the blocking of the tertiary amine with H^+ and the transformation of the catechol with H_2O_2 should recover fluorescence in an AND logical manner (Fig. 3). The latter transformation gives rise to an *o*-quinone which can potentially serve as an electron acceptor (like pyridine units do[270]) in a PET process involving the fluorophore but this does not appear to participate. The biological upshot is that H_2O_2 (stimulated by lipopolysaccharide) within lysosomes becomes visible with the aid of AND gate **93** in glial cells. Rat brain slices and entire nematodes also yield some of their secrets concerning H_2O_2 and H^+ in this way.

94 (ref. 263) possesses a dinitrobenzenesulfonyl unit which is a PET acceptor and whose PET accepting component can be displaced selectively by a soft nucleophile like glutathione so that its PET process is eliminated. Its use in this manner has been known since 2005.[271] **94** also contains an arylboronate unit which can be oxidized to a phenolate so

that a well-delocalized fluorophore of the fluorescein type is produced. Its use in this manner is also known.[272] It is very interesting to note another case where these same two units are reported in two different fluorescent molecules for separately detecting H_2O_2 and glutathione within a single 2018 publication.[273] However, it is the combination of these two units within **94** which allows AND logic (Fig. 3) to emerge. When **94** is inside macrophage cells, it responds with 'high' fluorescence when exposed to external glutathione and an external ONO_2^- donor. The same response is found when ONO_2^- is stimulated in macrophages by application of lipopolysaccharide and when glutathione is stimulated with caffeic acid treatment.

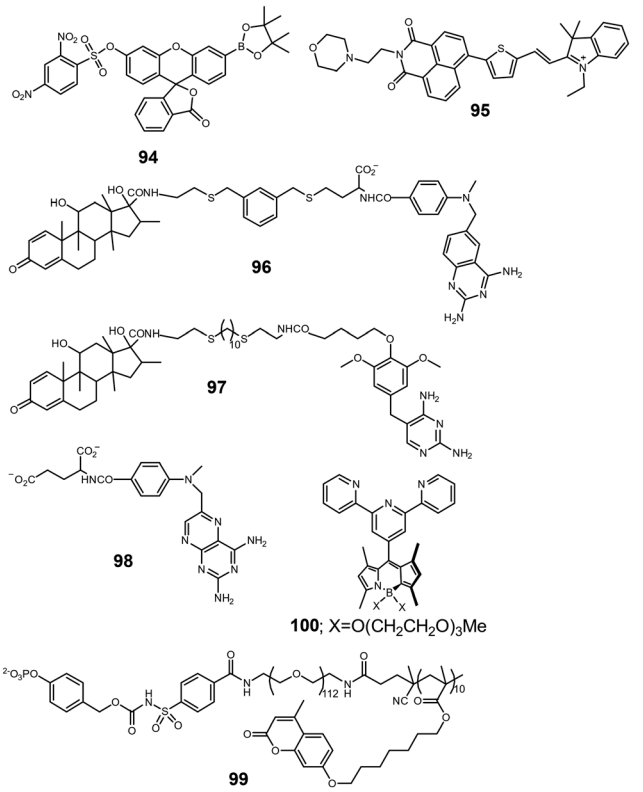

Continuing the recent successes of detecting the coincidence of key players[14] in small biospaces, **95** detects HSO_3^- and H^+ in lysosomes.[274] An amine side-chain provides the site for protonation and lysosome localization, as well as for PET donation. Popular lysosome sensors employ this design.[2] A hemicyanine provides an electron-poor alkene for Michael addition by HSO_3^- and also presents an easily rotatable double bond for de-excitation of the excited state. Thus, **95** has two separate sites with different pathways for excited state deactivation to out-compete fluorescence emission. Each of these pathways needs to be blocked by the appropriate input. The PET pathway from the amine is stopped by arrival of H^+ to bind the amine and the double bond pathway is removed entirely by the Michael addition. Green fluorescence emerges as the output in an AND logical fashion from the inputs of HSO_3^- and H^+.

Although intracellular logic operations based on small molecules is available in good numbers, persuading DNA devices to do the same has celebrity value even though intracellular nucleases are an ever-present hazard.[275–279] For instance, a combination of 2′-OMe substituted RNA and phosphorothioate bonds are used to protect the device and inputs within mammalian cells during the construction of an OR gate[277] whose operation is schematized in Fig. 20. Although based on toehold-mediated strand displacement,[135] a four-way strand exchange is employed here to avoid interference by endogenous oligonucleotides. On its own, the device has 'low' fluorescence since the fluorophore has a good quencher for a neighbour. When either $input_1$ or $input_2$ arrives, the device evolves to products where the fluorophore and the quencher exist of separate double strands, so that the fluorescence changes to 'high'. Application of both inputs to the device results in a competition where it doesn't matter who wins since the fluorescence will be 'high' either way. Rather similar, but extracellular, operations achieve two-input AND logic[280] or a half-adder[281] irrespective of the structural complexity of the devices achieved with DNA origami.

A ribosome needs to bind messenger RNA so that the latter's information can be translated into proteins.[217] This process begins with the start codon, which is commonly the sequence AUG. The heart of the RNA logic device is composed of a ribosome binding site and a start codon which are covered up by a stem-loop construct[282] so that downstream protein (*e.g.* green fluorescent protein) translation is switched 'off'.[283] Upon applying suitable RNA inputs, these two sites can be exposed so that protein production is switched 'on' as the output. An advanced version of this is shown schematically in Fig. 21, where multiple sets of these two sites are present. Only one pair of sites need to be exposed for protein translation since any downstream sites are forced open once the ribosome has locked on and translation has begun.[284] According to the functional integration idea, this logic behaviour can be represented as in Fig. 22 containing 5 OR gates. Related riboregulator-based systems give rise to arrays with multiple AND or NOT gates as well.

MicroRNAs bind to messenger RNA and so these can form an input-device pair. In the current implementation,[285] human cells are transfected with two pieces of messenger RNA, one coding for a RNA binding protein (L7Ae) while carrying several microRNA target regions and another coding for green fluorescent protein while carrying a L7Ae binding site. L7Ae's interaction with the messenger RNA stops its translation to the green fluorescent protein output. Thus, the microRNA's interaction with the device switches the green fluorescence 'on' (YES logic) by preventing expression of L7Ae. By employing target regions for two microRNAs, either input will block production of L7Ae in order for the fluorescence output to switch 'on' in an OR logical manner. Other two- (or three-) input gates are created in analogous ways. It is to be noted that RNA-based devices avoid the worry

of unwitting incorporation into the cell's own genome that DNA devices have to face.

Since complexity is common in cellular processes, rather complicated logic gate arrays can be discerned where the device consists of intracellular nucleic acids and proteins acting in concert. For instance, the two components of a transcription activation apparatus are separated within a yeast system, but they can be brought together to transcribe the lacZ gene which leads to synthesis of β-galactosidase – a measurable output.[286] The components which need to be brought together are the DNA binding protein (LexA) and a transcription activator (B42). If LexA is fused to dihydrofolate reductase (DHFR), the latter can be bound to the ligand methotrexate. If B42 is fused to the glucocorticoid receptor (GR), the latter can be bound to dexamethasone. So a dexamethasone–methotrexate construct[287] (**96**) is the final piece which solves the puzzle. A dexamethasone–trimethoprim construct[288] (**97**) works just as well since trimethoprim and methotrexate share a diaminopyrimidine motif. The process can be arrested by adding methotrexate itself (**98**) since it competes for the site of DHFR. The yeast system is also controlled by the promoter GAL1, which itself is activated by galactose but inhibited by glucose. So, we have a device driven by five inputs: **96**–**98**, galactose and glucose according to the logic array in Fig. 23.

Our final set of examples operate on the outside of living cells rather than inside but are still included in this section because of their cellular relevance and high novelty. **99** (ref. 289) is a diblock copolymeric nanoparticle where a sulfonamide ligand for the membrane-bound carbonic anhydrase IX is protected by *N*-acylation. Ultraviolet irradiation is used to dimerize the coumarin moieties so that a degree of cross-linking can be introduced to stabilize the nanoparticles. However, the protecting group can be removed with alkaline phosphatase *via* self-immolation[89] where a quinonemethide and CO_2 are eliminated. Thus the two proteins serve as inputs to allow entry, in an AND logical fashion,[88] of the nanoparticles into cells which overexpress

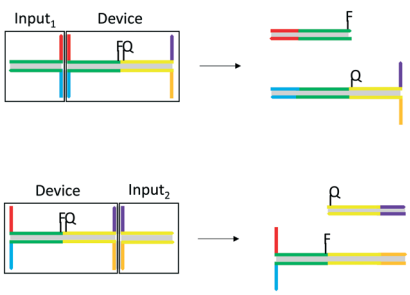

Fig. 20 Two-input OR logic gate[277] using four-way strand exchange based on toehold-mediated strand displacement. Complementary runs are shown in identical colours. Hybridized regions are shown in grey. F = fluorophore and Q = quencher (matched with F for efficient quenching *via* EET). The four-way strand exchange is clearly seen in the cross formed when the device and the input strands come together.

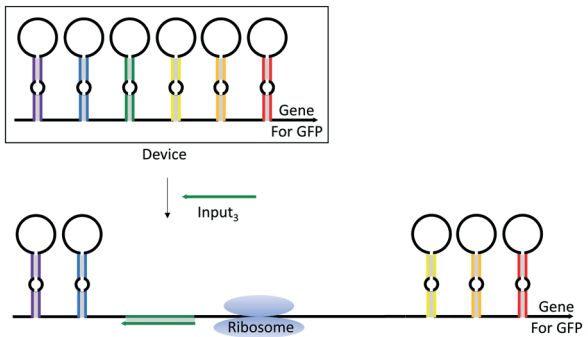

Fig. 21 Six-input logic gate array[284] based on RNA in *E. coli* producing green fluorescent protein (GFP) as output. An RNA strand ($input_3$) attacking the third stem-loop motif is illustrated. When the ribosome binding site and the AUG start codon are exposed at that location, the ribosome locks onto the device strand and moves to the right (relative to the strand) forcing open all the stem-loop motifs that it encounters until the GFP gene is reached so that GFP is generated.

both macromolecules on their surfaces. Such entry becomes more selective as a result.

The fluorescence of **100** (ref. 290) is switched 'off' when Zn^{2+} binds to make the terpyridine moiety more electron-poor and enable PET[57] from the BODIPY unit. However, a phosphate ligand would neutralize the effect of Zn^{2+} in **100**.Zn^{2+} to switch fluorescence back 'on'.[291] Another consequence of PET in this combination of orthogonally oriented pi-electron systems within the singlet excited state of **100**.Zn^{2+} is a charge recombination to give rise to the corresponding triplet excited state which is sufficiently long-lived to allow singlet oxygen generation for photodynamic therapy (PDT).[194] Human leukemia cells are triggered into apoptosis following PDT, which launches phosphatidyl serine from its normal position in the inner leaflet of the cell membrane to the outer leaflet. This exposed phosphate neutralizes the effect of Zn^{2+} in **100**.Zn^{2+} as discussed before. Therefore, PDT-caused cell apoptosis produces a diagnostic fluorescence 'on' signal and stops any further PDT at the same time. This is a 1 : 2 demultiplexer action (Fig. 13 and Table 5 previously shown in section 8) because the 'low' or 'high' status of an address input (phosphatidyl serine) is routing a data input (excitation light dose) into one or the other of two output lines (PDT or fluorescence).

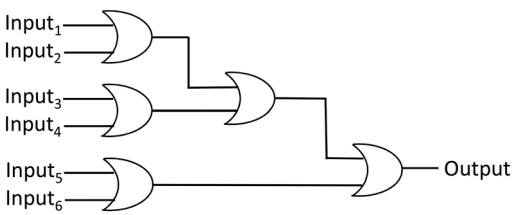

Fig. 22 Physical electronic representation of a 6-input logic gate array, which is found in the behaviour of a riboregulator-based RNA device.[284] Although all rows of the truth table are not tested, it is reasonably assumed that each input acts independently.

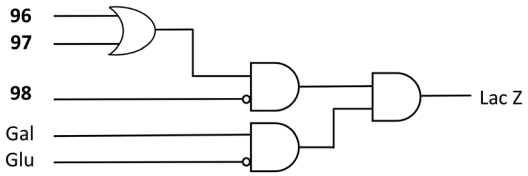

Fig. 23 Physical electronic representation of the logic array found in the behaviour of yeast system in ref. 286.

10. Conclusions

The developments of the past 5 years or so in molecular logic-based computation which are sampled here illustrate the vibrancy of the field. Boolean and other forms of logic are being employed to analyse (bio)chemical phenomena of various kinds by many, many laboratories around the world. Supramolecular agents, many of which are modular systems operating on some engineering principles, are running tasks with a significant degree of intelligence in areas as disparate as tracking biomarker combinations inside living cells and hiding communications akin to an enigma machine. SMARTI is occurring in all these situations. Fluorescent logic devices based on PET are among the clearest examples of molecular system design and engineering.

Conflicts of interest

There are no conflicts to declare.

Acknowledgements

We are grateful to the Leverhulme Trust (RPG-2019-314), China Scholarship Council, Queen's University Belfast, Department of Employment and Learning of Northern Ireland, G. M. Yao, F. F. Huang, Y. X. Lin and Q. Zhang for support and help.

References

1 G. Ashkenasy, T. M. Hermans, S. Otto and A. F. Taylor, *Chem. Soc. Rev.*, 2017, **46**, 2543.
2 A. P. de Silva and R. A. D. D. Rupasinghe, *J. Chem. Soc., Chem. Commun.*, 1985, 1669.
3 Y. C. Wang and H. Morawetz, *J. Am. Chem. Soc.*, 1976, **98**, 3611.
4 B. K. Selinger, *Aust. J. Chem.*, 1977, **30**, 2087.
5 G. S. Beddard, R. S. Davidson and T. D. Whelan, *Chem. Phys. Lett.*, 1978, **56**, 54.
6 H. Shizuka, M. Nakamura and T. Morita, *J. Phys. Chem.*, 1979, **83**, 2019.
7 H. Shizuka, T. Ogiwara and E. Kimura, *J. Phys. Chem.*, 1985, **89**, 4302.
8 J.-P. Konopelski, F. Kotzyba-Hibert, J.-M. Lehn, J.-P. Desvergne, F. Fages, A. Castellan and H. Bouas-Laurent, *J. Chem. Soc., Chem. Commun.*, 1985, 433.
9 G. Grynkiewicz, M. Poenie and R. Y. Tsien, *J. Biol. Chem.*, 1985, **206**, 3440.
10 A. P. de Silva and S. A. de Silva, *J. Chem. Soc., Chem. Commun.*, 1986, 1709.
11 M. E. Huston, K. W. Haider and A. W. Czarnik, *J. Am. Chem. Soc.*, 1988, **110**, 4460.
12 J.-M. Lehn, *Supramolecular Chemistry*, VCH, Weinheim, 1995.
13 V. Balzani and F. Scandola, *Supramolecular Photochemistry*, Ellis-Horwood, New York, 1991.
14 A. P. de Silva, H. Q. N. Gunaratne and C. P. McCoy, *Nature*, 1993, **364**, 42.
15 A. P. de Silva, *Molecular Logic-based Computation*, Royal Society of Chemistry, Cambridge, 2013.
16 *Molecular and Supramolecular Information Processing*, ed. E. Katz, Wiley-VCH, Weinheim, 2012.
17 *Biomolecular Information Processing*, ed. E. Katz, Wiley-VCH, Weinheim, 2012.
18 K. Szacilowski, *Infochemistry*, Wiley, Chichester, 2012.
19 V. Balzani, A. Credi and M. Venturi, *Molecular Devices and Machines*, VCH, Weinheim, 2nd edn, 2008.
20 *Enzyme-Based Computing Systems*, ed. E. Katz, Wiley-VCH, Weinheim, 2019.
21 A. P. de Silva, Y. Leydet, C. Lincheneau and N. D. McClenaghan, *J. Phys.: Condens. Matter*, 2006, **18**, S1847.
22 S. Uchiyama and A. P. de Silva, *Nat. Nanotechnol.*, 2007, **2**, 399.
23 E. Katz and V. Privman, *Chem. Soc. Rev.*, 2010, **39**, 1835.
24 J. Andreasson and U. Pischel, *Chem. Soc. Rev.*, 2015, **44**, 1053.
25 B. Daly, J. Ling, V. A. Silverson and A. P. de Silva, *Chem. Commun.*, 2015, **51**, 8403.
26 S. Erbas-Cakmak, S. Kolemen, A. C. Sedgwick, T. Gunnlaugsson, T. D. James, J. Y. Yoon and E. U. Akkaya, *Chem. Soc. Rev.*, 2018, **47**, 2228.
27 J. Andreasson and U. Pischel, *Chem. Soc. Rev.*, 2018, **47**, 2266.
28 A. Weller, *Pure Appl. Chem.*, 1968, **16**, 115.
29 R. A. Bissell, A. P. de Silva, H. Q. N. Gunaratne, P. L. M. Lynch, G. E. M. Maguire and K. R. A. S. Sandanayake, *Chem. Soc. Rev.*, 1992, **21**, 187.
30 A. P. de Silva, H. Q. N. Gunaratne, T. Gunnlaugsson, A. J. M. Huxley, C. P. McCoy, J. T. Rademacher and T. E. Rice, *Chem. Rev.*, 1997, **97**, 1515.
31 A. P. de Silva, T. P. Vance, M. E. S. West and G. D. Wright, *Org. Biomol. Chem.*, 2008, **6**, 2468.
32 A. P. de Silva, T. S. Moody and G. D. Wright, *Analyst*, 2009, **134**, 2385.
33 W. Zhang, Z. Ma, L. P. Du and M. Y. Li, *Analyst*, 2014, **139**, 2641.
34 B. Daly, J. Ling and A. P. de Silva, *Chem. Soc. Rev.*, 2015, **44**, 4203.
35 D. Wu, A. C. Sedgwick, T. Gunnlaugsson, E. U. Akkaya, J. Y. Yoon and T. D. James, *Chem. Soc. Rev.*, 2017, **46**, 7105.
36 A. P. de Silva and S. Uchiyama, *Top. Curr. Chem.*, 2011, **300**, 1.
37 A. P. de Silva, S. A. de Silva, A. S. Dissanayake and K. R. A. S. Sandanayake, *J. Chem. Soc., Chem. Commun.*, 1989, 1054.
38 A. P. Malvino and J. A. Brown, *Digital Computer Electronics*, Glencoe, Lake Forest, 3rd edn, 1993.

39 A. Dorlars, C.-W. Schellhammer and J. Schroeder, *Angew. Chem., Int. Ed. Engl.*, 1975, **14**, 665.
40 B. M. Krasovitski and B. M. Bolotin, *Organic Luminescent Materials*, VCH, Weinheim, 1988.
41 S. Uchiyama, E. Fukatsu, G. D. McClean and A. P. de Silva, *Angew. Chem., Int. Ed.*, 2016, **55**, 768.
42 *Electron Transfer in Chemistry*, ed. V. Balzani, P. Piotrowiak, M. A. J. Rodgers, J. Mattay, D. Astruc, H. B. Gray, J. Winkler, S. Fukuzumi, T. E. Mallouk, Y. Haas, A. P. de Silva and I. Gould, Wiley-VCH, Weinheim, 2001.
43 R. A. Bissell, A. P. de Silva, W. T. M. L. Fernando, S. T. Patuwathavithana and T. K. S. D. Samarasinghe, *Tetrahedron Lett.*, 1991, **32**, 425.
44 C. K. Mann and K. K. Barnes, *Electrochemical Reactions in Non-aqueous Solvents*, Dekker, New York, 1970.
45 F. Pragst and F. G. Weber, *J. Prakt. Chem.*, 1976, **318**, 51.
46 L. Meites and P. Zuman, *Electrochemical Data, Part 1*, Wiley, New York, 1974, vol. IA.
47 R. A. Marcus,https://www.nobelprize.org/prizes/chemistry/1992/marcus/lecture.
48 W. J. Chi, J. Chen, W. J. Liu, C. Wang, Q. K. Qi, Q. L. Qiao, T. M. Tan, K. M. Xiong, X. Liu, K. G. Kang, Y.-T. Chang, Z. C. Xu and X. G. Liu, *J. Am. Chem. Soc.*, 2020, **142**, 6777.
49 L. P. Hammett, *Physical Organic Chemistry*, McGraw Hill, New York, 2nd edn, 1970.
50 E. V. Anslyn and D. A. Dougherty, *Modern Physical Organic Chemistry*, University Science Books, Mill Valley, 2005.
51 R. Zammit, M. Pappova, E. Zammit, J. Gabarretta and D. C. Magri, *Can. J. Chem.*, 2015, **93**, 199.
52 G. J. Scerri, M. Cini, J. S. Schembri, P. Fontoura da Costa, A. D. Johnson and D. C. Magri, *ChemPhysChem*, 2017, **18**, 1742.
53 R. Mathew, R. R. Mallia, S. Haridas and J. P. Jacob, *J. Photochem. Photobiol., A*, 2020, **397**, 112552.
54 A. P. de Silva, S. S. K. de Silva, N. C. W. Goonesekera, H. Q. N. Gunaratne, P. L. M. Lynch, K. R. Nesbitt, S. T. Patuwathavithana and N. L. D. S. Ramyalal, *J. Am. Chem. Soc.*, 2007, **129**, 3050.
55 A. P. de Silva and H. Q. N. Gunaratne, *J. Chem. Soc., Chem. Commun.*, 1990, 186.
56 A. P. de Silva, H. Q. N. Gunaratne and G. E. M. Maguire, *J. Chem. Soc., Chem. Commun.*, 1994, 1213.
57 A. P. de Silva, I. M. Dixon, H. Q. N. Gunaratne, T. Gunnlaugsson, P. R. S. Maxwell and T. E. Rice, *J. Am. Chem. Soc.*, 1999, **121**, 1393.
58 D. C. Magri, G. J. Brown, G. D. McClean and A. P. de Silva, *J. Am. Chem. Soc.*, 2006, **128**, 4950.
59 A. P. de Silva, C. M. Dobbin, T. P. Vance and B. Wannalerse, *Chem. Commun.*, 2009, 1386.
60 E. Hughes, *Electrical Technology*, Longman, Burnt Mill, 6th edn, 1990.
61 N. A. C. Bakker, P. G. Wiering, A. M. Brouwer, J. M. Warman and J. W. Verhoeven, *Mol. Cryst. Liq. Cryst.*, 1990, **183**, 31.
62 A. Bachtold, P. Hadley, T. Nakanishi and C. Dekker, *Science*, 2001, **294**, 1317.
63 H. Song, Y. Kim, Y. H. Jang, H. Jeong, M. A. Reed and T. Lee, *Nature*, 2009, **462**, 1039.
64 A. E. Keirstead, J. W. Bridgewater, Y. Terazono, G. Kodis, S. Straight, P. A. Liddell, A. L. Moore, T. A. Moore and D. Gust, *J. Am. Chem. Soc.*, 2010, **132**, 6588.
65 A. J. M. Huxley, M. Schroeder, H. Q. N. Gunaratne and A. P. de Silva, *Angew. Chem., Int. Ed.*, 2014, **53**, 3622.
66 Y. Hirshberg, *J. Am. Chem. Soc.*, 1956, **78**, 2304.
67 P. Remon, S. M. Li, M. Grotli, U. Pischel and J. Andreasson, *Chem. Commun.*, 2016, **52**, 4659.
68 A. P. de Silva, H. Q. N. Gunaratne, P. L. M. Lynch, A. L. Patty and G. L. Spence, *J. Chem. Soc., Perkin Trans. 2*, 1993, 1611.
69 F. M. Raymo and S. Giordani, *J. Am. Chem. Soc.*, 2001, **123**, 4651.
70 M. Hammarson, J. R. Nilsson, S. M. Li, T. Beke-Somfai and J. Andreasson, *J. Phys. Chem. B*, 2013, **117**, 13561.
71 D. Nilsson, N. Robinson, M. Berggren and R. Forchheimer, *Adv. Mater.*, 2005, **17**, 353.
72 M. Pars, C. C. Hofmann, K. Willinger, P. Bauer, M. Thelakkat and J. Kohler, *Angew. Chem., Int. Ed.*, 2011, **50**, 11405.
73 C. Li, H. Yan, L.-X. Zhao, G.-F. Zhang, Z. Hu, Z.-L. Huang and M.-Q. Zhu, *Nat. Commun.*, 2014, **5**, 5709.
74 I. Gallardo, G. Guirado, J. Hernando, S. Morais and G. Prats, *Chem. Sci.*, 2016, **7**, 1819.
75 J. M. A. Spiteri, C. J. Mallia, G. J. Scerri and D. C. Magri, *Org. Biomol. Chem.*, 2017, **15**, 10116.
76 A. Diacono, M. C. Aquilina, A. Calleja, G. Agius, G. Gauci, K. Szaciłowski and D. C. Magri, *Org. Biomol. Chem.*, 2020, **18**, 4773.
77 A. P. de Silva, H. Q. N. Gunaratne and C. P. McCoy, *J. Am. Chem. Soc.*, 1997, **119**, 7891.
78 D. C. Magri and J. C. Spiteri, *Org. Biomol. Chem.*, 2017, **15**, 6706.
79 R. A. Schultz, B. D. White, D. M. Dishong, K. A. Arnold and G. W. Gokel, *J. Am. Chem. Soc.*, 1985, **107**, 6659.
80 L. X. Lu, C. X. Chen, D. Zhao, J. Sun and X. R. Yang, *Anal. Chem.*, 2016, **88**, 1238.
81 F. S. Richardson, *Chem. Rev.*, 1982, **82**, 541.
82 D. Parker, *Chem. Soc. Rev.*, 2004, **33**, 156.
83 A. P. de Silva, H. Q. N. Gunaratne and T. E. Rice, *Angew. Chem., Int. Ed. Engl.*, 1996, **35**, 2116.
84 A. P. de Silva, H. Q. N. Gunaratne, T. E. Rice and S. Stewart, *Chem. Commun.*, 1997, 1891.
85 S. J. Butler and D. Parker, *Chem. Soc. Rev.*, 2013, **42**, 1652.
86 C. X. Yin, F. J. Huo, N. P. Cooley, D. Spencer, K. Bartholomew, C. L. Barnes and T. E. Glass, *ACS Chem. Neurosci.*, 2017, **8**, 1159.
87 K. Kalyanasundaram and J. K. Thomas, *J. Phys. Chem.*, 1977, **81**, 2176.
88 S. Debieu and A. Romieu, *Org. Biomol. Chem.*, 2015, **13**, 10348.
89 R. J. Amir, N. Pessah, M. Shamis and N. Shabat, *Angew. Chem., Int. Ed.*, 2003, **42**, 4494.
90 E. Vander Donckt, *Prog. React. Kinet.*, 1970, **5**, 273.

91 B. Valeur and M. N. Berberan-Santos, *Molecular Fluorescence: Principles and Applications*, Wiley-VCH, Weinheim, 2nd edn, 2012.
92 P. R. Ashton, I. Baxter, S. J. Cantrill, M. C. T. Fyfe, P. T. Glink, J. F. Stoddart, A. J. P. White and D. J. Williams, *Angew. Chem., Int. Ed.*, 1998, **37**, 1294.
93 A. Wolf, E. Moulin, J.-J. Cid, A. Goujon, G. Y. Du, E. Busseron, G. Fuks and N. Giuseppone, *Chem. Commun.*, 2015, **51**, 4212.
94 E. Moulin, F. Niess, M. Maaloum, E. Buhler, I. Nyrkova and N. Giuseppone, *Angew. Chem., Int. Ed.*, 2010, **49**, 6974.
95 M. C. Jimenez-Molero, C. Dietrich-Buchecker and J.-P. Sauvage, *Chem. Commun.*, 2003, 1613.
96 Z. Dadon, M. Samiappan, E. Yishay and G. Ashkenasy, *Chem. – Eur. J.*, 2010, **16**, 12096.
97 C. S. Wood, T. K. Ronson, A. J. McConnell, D. A. Roberts and J. R. Nitschke, *Chem. Sci.*, 2016, **7**, 1702.
98 M. Yoshizawa, M. Tamura and M. Fujita, *J. Am. Chem. Soc.*, 2004, **126**, 6846.
99 N. Zhang, W.-Y. Lo, A. Jose, Z. X. Cai, L. W. Li and L. P. Yu, *Adv. Mater.*, 2017, **29**, 1701248.
100 M. Irie, *Chem. Rev.*, 2000, **100**, 1685.
101 L. W. Li, W. Y. Lo, Z. X. Cai, N. Zhang and L. P. Yu, *Chem. Sci.*, 2016, **7**, 3137.
102 F. B. Meng, Y.-M. Hervault, Q. Shao, B. H. Hu, L. Norel, S. Rigaut and X. D. Chen, *Nat. Commun.*, 2014, **5**, 3023.
103 U. Pischel and J. Andreasson, *New J. Chem.*, 2010, **34**, 2701.
104 H. Kuhn, *Pure Appl. Chem.*, 1981, **53**, 2105.
105 M. Frigoli and G. H. Mehl, *Angew. Chem., Int. Ed.*, 2005, **44**, 5048.
106 M. M. Lerch, M. J. Hansen, W. A. Velema, W. Szymanski and B. L. Feringa, *Nat. Commun.*, 2016, **7**, 12054.
107 F.-Y. Tang, J.-N. Hou, K. X. Liang, Y. Liu, L. Deng and Y.-N. Liu, *New J. Chem.*, 2017, **41**, 6071.
108 S. Helmy, F. A. Leibfarth, S. Oh, J. E. Poelma, C. J. Hawker and J. Read de Alaniz, *J. Am. Chem. Soc.*, 2014, **136**, 8169.
109 V. R. de la Rosa, Z. Y. Zhang, B. G. De Geest and R. Hoogenboom, *Adv. Funct. Mater.*, 2015, **25**, 2511.
110 R. Elghanian, J. Storhoff, R. C. Mucic, R. L. Letsinger and C. A. Mirkin, *Science*, 1997, **277**, 1078.
111 F. M. Winnik, *Macromolecules*, 1990, **23**, 233.
112 S. Uchiyama, Y. Matsumura, A. P. de Silva and K. Iwai, *Anal. Chem.*, 2003, **75**, 5926.
113 S. Uchiyama, N. Kawai, A. P. de Silva and K. Iwai, *J. Am. Chem. Soc.*, 2004, **126**, 3032.
114 Y. L. Xianyu, Z. Wang, J. S. Sun, X. F. Wang and X. Y. Jiang, *Small*, 2014, **10**, 4833.
115 J. H. Chen, Z. Y. Fang, P. C. Lie and L. W. Zeng, *Anal. Chem.*, 2012, **84**, 6321.
116 M. Prakash and N. Gershenfeld, *Science*, 2007, **315**, 832.
117 C. Amatore, L. Thouin and J.-S. Warkocz, *Chem. – Eur. J.*, 1999, **5**, 456.
118 K. Szaciłowski, W. Macyk and G. Stochel, *J. Am. Chem. Soc.*, 2006, **128**, 4550.
119 W. Zhan and R. M. Crooks, *J. Am. Chem. Soc.*, 2003, **125**, 9934.
120 O. Steinbock, P. Kettunen and K. Showalter, *J. Phys. Chem.*, 1996, **100**, 18970.
121 A. Adamatzky, *Philos. Trans. R. Soc., A*, 2015, **373**, 20140216.
122 G. Loget, G. Z. Li and B. Fabre, *Chem. Commun.*, 2015, **51**, 11115.
123 C. R. Yang, D. Zou, J. C. Chen, L. Y. Zhang, J. R. Miao, D. Huang, Y. Y. Du, S. Yang, Q. F. Yang and Y. L. Tang, *Chem. – Eur. J.*, 2018, **24**, 4019.
124 A. P. de Silva and N. D. McClenaghan, *J. Am. Chem. Soc.*, 2000, **122**, 3965.
125 J. Andreasson, S. D. Straight, T. A. Moore, A. L. Moore and D. Gust, *J. Am. Chem. Soc.*, 2008, **130**, 11122.
126 P. Ceroni, G. Bergamini and V. Balzani, *Angew. Chem., Int. Ed.*, 2009, **48**, 8516.
127 H. Li, Y. Liu, S. Dong and E. Wang, *NPG Asia Mater.*, 2015, **7**, e166.
128 P. Singh, H. Singh, G. Bhargava and S. Kumar, *Sens. Actuators, B*, 2017, **245**, 1004.
129 Y. Lvov, G. Decher and H. Mohwald, *Langmuir*, 1993, **9**, 481.
130 H. Kuhn, *Pure Appl. Chem.*, 1965, **11**, 345.
131 J. F. Yu, Q. Wang, D. O'Hare and L. Y. Sun, *Chem. Soc. Rev.*, 2017, **46**, 5950.
132 W. Y. Shi, Y. Fu, Z. X. Li and M. Wei, *Chem. Commun.*, 2015, **51**, 711.
133 G. Boole, *An Investigation of the Laws of Thought*, Dover, New York, 1958.
134 V. Derycke, R. Martel, J. Appenzeller and P. Avouris, *Nano Lett.*, 2001, **1**, 453.
135 G. Seelig, D. Soloveichik, D. Y. Zhang and E. Winfree, *Science*, 2006, **314**, 1585.
136 J. Andreasson, S. D. Straight, T. A. Moore, A. L. Moore and D. Gust, *J. Am. Chem. Soc.*, 2008, **130**, 11122.
137 P. Ceroni, G. Bergamini and V. Balzani, *Angew. Chem., Int. Ed.*, 2009, **48**, 8516.
138 H. M. Yao, J. W. Wang, H. Chen, X. F. Mei, Z. Su, J. N. Wu, Z. H. Lin and Q. D. Ling, *RSC Adv.*, 2017, **7**, 12161.
139 C. R. Yang, S. Yang, L. B. Song, Y. Yao, X. Lin, K. C. Cai, Q. F. Yang and Y. L. Tang, *Chem. Commun.*, 2019, **55**, 8005.
140 L. G. Shapiro and G. C. Stockman, *Computer Vision*, Prentice-Hall, Upper Saddle River, NJ, 2001.
141 *How animals see the world*, ed. O. F. Lazareva, T. Shimizu and E. A. Wasserman, Oxford University Press, Oxford, 2012.
142 J. Ling, G. W. Naren, J. Kelly, T. S. Moody and A. P. de Silva, *J. Am. Chem. Soc.*, 2015, **137**, 3763.
143 J. L. Dektar and N. P. Hacker, *J. Am. Chem. Soc.*, 1990, **112**, 6004.
144 S. A. de Silva, A. Zavaleta, D. E. Baron, O. Allam, E. Isidor, N. Kashimura and J. M. Percarpio, *Tetrahedron Lett.*, 1997, **38**, 2237.
145 A. P. de Silva, H. Q. N. Gunaratne and C. P. McCoy, *Chem. Commun.*, 1996, 2399.
146 J. J. Tabor, H. M. Salis, Z. B. Simpson, A. A. Chevalier, A. Levskaya, E. M. Marcotte, C. A. Voigt and A. D. Ellington, *Cell*, 2009, **137**, 1272.
147 S. M. Chirieleison, P. B. Allen, Z. B. Simpson, A. D. Ellington and X. Chen, *Nat. Chem.*, 2013, **5**, 1000.

148 J. Ling, G. W. Naren, J. Kelly, D. B. Fox and A. P. de Silva, *Chem. Sci.*, 2015, **6**, 4472.
149 B. Hayes, *Am. Sci.*, 2001, **89**, 490.
150 R. W. Keyes, *Rev. Mod. Phys.*, 1989, **61**, 279.
151 C. Y. Yao, J. Ling, L. Y. H. Chen and A. P. de Silva, *Chem. Sci.*, 2019, **10**, 2272.
152 A. P. de Silva, M. R. James, B. O. F. McKinney, D. A. Pears and S. M. Weir, *Nat. Mater.*, 2006, **5**, 787.
153 B. O. F. McKinney, B. Daly, C. Y. Yao, M. Schroeder and A. P. de Silva, *ChemPhysChem*, 2017, **18**, 1760.
154 T. Ratner, O. Reany and E. Keinan, *ChemPhysChem*, 2009, **10**, 3303.
155 A. Casula, P. Begines, A. Bettoschi, J. G. Fernandez-Bolanos, F. Isaia, V. Lippolis, O. Lopez, G. Picci, M. A. Scorciapino and C. Caltagirone, *Chem. Commun.*, 2017, **53**, 11869.
156 J. M. Ottaway, in *Indicators*, ed. E. Bishop, Pergamon, London, 1972, p. 469.
157 E. Banyay, in *Indicators*, ed. E. Bishop, Pergamon, London, 1972, p. 65.
158 L. Zang, R. C. Liu, M. W. Holman, K. T. Nguyen and D. M. Adams, *J. Am. Chem. Soc.*, 2002, **124**, 10640.
159 D. P. Kennedy, C. M. Kormos and S. C. Burdette, *J. Am. Chem. Soc.*, 2009, **131**, 8578.
160 A. D. Johnson, K. A. Paterson, J. C. Spiteri, S. A. Denisov, G. Jonusauskas, A. Tron, N. D. McClenaghan and D. C. Magri, *New J. Chem.*, 2016, **40**, 9917.
161 G. J. Scerri, J. C. Spiteri, C. J. Mallia and D. C. Magri, *Chem. Commun.*, 2019, **55**, 4961.
162 S. R. Bhatta, V. Bheemireddy and A. Thakur, *Organometallics*, 2017, **36**, 829.
163 M. Li, Z. Q. Guo, W. H. Zhu, F. Marken and T. D. James, *Chem. Commun.*, 2015, **51**, 1293.
164 M. de Sousa, B. de Castro, S. Abad, M. A. Miranda and U. Pischel, *Chem. Commun.*, 2006, 2051.
165 J. M. Montenegro, E. Perez-Inestrosa, D. Collado, Y. Vida and R. Suau, *Org. Lett.*, 2004, **6**, 2353.
166 S. Alves, F. Pina, M. T. Albelda, E. Garcia-Espana, C. Soriano and S. V. Luis, *Eur. J. Inorg. Chem.*, 2001, 405.
167 A. E. G. Cass, G. Davis, G. D. Francis, H. A. O. Hill, W. J. Aston, I. J. Higgins, E. V. Plotkin, L. D. Scott and A. P. F. Turner, *Anal. Chem.*, 1984, **56**, 667.
168 S. Liu, L. Wang, W. J. Lian, H. Y. Liu and C.-Z. Li, *Chem. – Asian J.*, 2015, **10**, 225.
169 D. Margulies, C. E. Felder, G. Melman and A. Shanzer, *J. Am. Chem. Soc.*, 2007, **129**, 347.
170 O. Lustgarten, L. Motiei and D. Margulies, *ChemPhysChem*, 2017, **18**, 1678.
171 J. Andreasson and U. Pischel, *Chem. Soc. Rev.*, 2018, **47**, 2266.
172 A. Schonberg, *Preparative Organic Photochemistry*, Springer, Berlin, 1968.
173 C. P. Carvalho, Z. Domınguez, J. P. Da Silva and U. Pischel, *Chem. Commun.*, 2015, **51**, 2698.
174 F. Pina, M. J. Melo, M. Maestri, P. Passaniti and V. Balzani, *J. Am. Chem. Soc.*, 2000, **122**, 4496.
175 M. C. Moncada, A. J. Parola, C. Lodeiro, F. Pina, M. Maestri and V. Balzani, *Chem. – Eur. J.*, 2004, **10**, 1519.
176 F. Kink, M. P. Collado, S. Wiedbrauk, P. Mayer and H. Dube, *Chem. – Eur. J.*, 2017, **23**, 6237.
177 A. Credi, V. Balzani, S. J. Langford and J. F. Stoddart, *J. Am. Chem. Soc.*, 1997, **119**, 2679.
178 A. J. Bryan, A. P. de Silva, S. A. de Silva, R. A. D. D. Rupasinghe and K. R. A. S. Sandanayake, *Biosensors*, 1989, **4**, 169.
179 M. Orrit and J. Bernard, *Phys. Rev. Lett.*, 1990, **65**, 2716.
180 E. Betzig and R. J. Chichester, *Science*, 1993, **262**, 1422.
181 X. S. Xie, *Acc. Chem. Res.*, 1996, **29**, 598.
182 W. E. Moerner and L. Kador, *Phys. Rev. Lett.*, 1989, **62**, 2535.
183 M. Elstner, K. Weisshart, K. Müllen and A. Schiller, *J. Am. Chem. Soc.*, 2012, **134**, 8098.
184 J. B. Liu, H. N. Ji, J. Huang, L. Li, Q. Wang, X. H. Yang and K. M. Wang, *ChemistrySelect*, 2016, **3**, 347.
185 S. Brasselet and W. E. Moerner, *Single Mol.*, 2000, **1**, 17.
186 L. Zang, R. Liu, M. W. Holman, K. T. Nguyen and D. M. Adams, *J. Am. Chem. Soc.*, 2002, **124**, 10640.
187 M. W. Holman, R. C. Liu, L. Zang, P. Yan, S. A. DiBenedetto, R. D. Bowers and D. M. Adams, *J. Am. Chem. Soc.*, 2004, **126**, 16126.
188 B. Rout, *Sci. Rep.*, 2016, **6**, 27115.
189 B. Rout and P. L. Bigliardi, *Synlett*, 2017, **28**, 1005.
190 J. B. Birks, *Photophysics of Aromatic Molecules*, Wiley, London, 1970.
191 N. J. Turro, V. Ramamurthy and J. C. Scaiano, *Modern Molecular Photochemistry of Organic Molecules*, University Science Books, Sausalito, 2010.
192 L. R. Milgrom, *The Colours of Life: An Introduction to the Chemistry of Porphyrins and Related Compounds*, Oxford University Press, Oxford, 2001.
193 *Chemometrics: Mathematics and Statistics in Chemistry*, ed. B. R. Kowalski, Springer, Dordrecht, 1984.
194 R. Bonnett, *Chemical Aspects of Photodynamic Therapy*, Gordon and Breach, Amsterdam, 2000.
195 T. Sarkar, K. Selvakumar, L. Motiei and D. Margulies, *Nat. Commun.*, 2016, **7**, 11374.
196 B. Rout, L. Unger, G. Armony, M. A. Iron and D. Margulies, *Angew. Chem., Int. Ed.*, 2012, **51**, 12477.
197 J. Hatai, L. Motiei and D. Margulies, *J. Am. Chem. Soc.*, 2017, **139**, 2136.
198 O. Lustgarten, R. Carmieli, L. Motiei and D. Margulies, *Angew. Chem., Int. Ed.*, 2019, **58**, 184.
199 D. M. J. Lilley, *Q. Rev. Biophys.*, 2000, **33**, 109.
200 N. Biggs, *Codes: An introduction to Information Communication and Cryptography*, Springer, London, 2008.
201 A. C. Boukis, K. Reiter, M. Frölich, D. Hofheinz and M. A. R. Meier, *Nat. Commun.*, 2018, **9**, 1439.
202 I. K. Ugi, *Angew. Chem., Int. Ed. Engl.*, 1962, **1**, 8.
203 W. Zhang and D. P. Curran, *Tetrahedron*, 2006, **62**, 11837.
204 Smith Kline Beecham Corp, *US Pat.*, 6,210,900 B1, 3 April 2001.
205 M. Vella Refalo, J. C. Spiteri and D. C. Magri, *New J. Chem.*, 2018, **42**, 16474.
206 M. Vella Refalo, N. V. Farrugia, A. D. Johnson, S. Klejna, K. Szaciłowski and D. C. Magri, *J. Mater. Chem. C*, 2019, **7**, 15225.

207 H. Komatsu, S. Matsumoto, S.-I. Tamaru, K. Kaneko, M. Ikeda and I. Hamachi, *J. Am. Chem. Soc.*, 2009, **131**, 5580.
208 M. Ikeda, T. Tanida, T. Yoshii, K. Kurotani, S. Onogi, K. Urayama and I. Hamachi, *Nat. Chem.*, 2014, **6**, 511.
209 T. Soboleva, H. J. Esquer, A. D. Benninghoff and L. M. Berreau, *J. Am. Chem. Soc.*, 2017, **139**, 9435.
210 U. G. Reddy, J. Axthelm, P. Hoffmann, N. Taye, S. Glaser, H. Gorls, S. L. Hopkins, W. Plass, U. Neugebauer, S. Bonnet and A. Schiller, *J. Am. Chem. Soc.*, 2017, **139**, 4991.
211 I. S. Turan, G. Gunaydin, S. Ayan and E. U. Akkaya, *Nat. Commun.*, 2018, **9**, 805.
212 X. Zhang and S. Soh, *Adv. Mater.*, 2017, **29**, 1606483.
213 K. P. Zauner and M. Conrad, *Biotechnol. Prog.*, 2001, **17**, 553.
214 F. M. Raymo and S. Giordani, *Proc. Natl. Acad. Sci. U. S. A.*, 2002, **99**, 4941.
215 K. Szacilowski, *Chem. – Eur. J.*, 2004, **10**, 2520.
216 B. A. Badeau, M. P. Comerford, C. K. Arakawa, J. A. Shadish and C. A. DeForest, *Nat. Chem.*, 2018, **10**, 251.
217 J. M. Berg, L. Stryer, J. Tymoczko and G. Gatto, *Biochemistry*, Freeman, San Francisco, 9th edn, 2019.
218 H. Nagase and G. B. Fields, *Pept. Sci.*, 1996, **40**, 399.
219 B. Daly, T. S. Moody, A. J. M. Huxley, C. Y. Yao, B. Schazmann, A. Alves-Areias, J. F. Malone, H. Q. N. Gunaratne, P. Nockemann and A. P. de Silva, *Nat. Commun.*, 2019, **10**, 49.
220 F. Diederich, *Cyclophanes*, Royal Society of Chemistry, Cambridge, 1991.
221 L. M. Adleman, *Science*, 1994, **266**, 1021.
222 J. C. Cox, D. S. Cohen and A. D. Ellington, *Trends Biotechnol.*, 1999, **17**, 151.
223 X. Chen and A. D. Ellington, *Curr. Opin. Biotechnol.*, 2010, **21**, 392.
224 H. J. Liu, J. B. Wang, S. P. Song, C. H. Fan and K. V. Gothelf, *Nat. Commun.*, 2015, **6**, 10089.
225 M. N. Stojanovic, T. E. Mitchell and D. Stefanovic, *J. Am. Chem. Soc.*, 2002, **124**, 3555.
226 A. Saghatelian, N. H. Volcker, K. M. Guckian, V. S. Y. Lin and M. R. Ghadiri, *J. Am. Chem. Soc.*, 2003, **125**, 346.
227 A. Okamoto, K. Tanaka and I. Saito, *J. Am. Chem. Soc.*, 2004, **126**, 9458.
228 J. Macdonald, D. Stefanovic and M. N. Stojanovic, *Sci. Am.*, 2008, **299**(5), 84.
229 M. N. Stojanovic, D. Stefanovic and S. Rudchenko, *Acc. Chem. Res.*, 2014, **47**, 1845.
230 R. Orbach, F. Remacle, R. D. Levine and I. Willner, *Chem. Sci.*, 2014, **5**, 1074.
231 R. Orbach, B. Willner and I. Willner, *Chem. Commun.*, 2015, **51**, 4144.
232 Y. L. Zhang, W. H. Chen, X. T. Dong, H. Fan, X. H. Wang and L. J. Bian, *Sens. Actuators, B*, 2018, **261**, 58.
233 R.-R. Gao, T.-M. Yao, X.-Y. Lv, Y.-Y. Zhu, Y.-W. Zhang and S. Shi, *Chem. Sci.*, 2017, **8**, 4211.
234 Y. Benenson, B. Gil, U. Ben-Dor, R. Adar and E. Shapiro, *Nature*, 2004, **429**, 423.
235 M. N. Stojanovic and D. Stefanovic, *Nat. Biotechnol.*, 2003, **21**, 1069.
236 A. R. Chandrasekaran, *ACS Synth. Biol.*, 2020, **9**, 1490.
237 R. P. Connelly, E. S. Morozkin and Y. V. Gerasimova, *ChemBioChem*, 2018, **19**, 203.
238 M. Balter, S. Li, J. R. Nilsson, J. Andreasson and U. Pischel, *J. Am. Chem. Soc.*, 2013, **135**, 10230.
239 D. Q. Fan, E. K. Wang and S. J. Dong, *ACS Appl. Mater. Interfaces*, 2017, **9**, 1322.
240 M. Wang, G. X. Zhang and D. Q. Zhang, *Chem. Commun.*, 2015, **51**, 3812.
241 C. Green and C. Tibbetts, *Nucleic Acids Res.*, 1981, **9**, 1905.
242 K. Nishijima and T. Nakakuki, *New Gener. Comput.*, 2020, **38**, 285.
243 A. Bader and S. L. Cockroft, *Chem. Commun.*, 2020, **56**, 5135.
244 L. Qian and E. Winfree, *J. R. Soc., Interface*, 2011, **8**, 1281.
245 L. Qian and E. Winfree, *Science*, 2011, **332**, 1196.
246 X. H. Huang and L. Tao, *J. Mater. Chem. C*, 2020, **8**, 821.
247 F. Wang, H. Lv, Q. Li, J. Li, X. L. Zhang, J. Y. Shi, L. H. Wang and C. H. Fan, *Nat. Commun.*, 2020, **11**, 121.
248 H. M. Su, J. L. Xu, Q. Wang, F. Wang and X. Zhou, *Nat. Commun.*, 2019, **10**, 5390.
249 T. Q. Song, A. Eshra, S. Shah, H. Bui, D. Fu, M. Yang, R. Mokhtar and J. Reif, *Nat. Nanotechnol.*, 2019, **14**, 1075.
250 C. Y. Zhou, H. M. Geng, P. F. Wang and C. L. Guo, *Small*, 2019, **15**, 1903489.
251 G. D. Wright, C. Y. Yao, T. S. Moody and A. P. de Silva, *Chem. Commun.*, 2020, **56**, 6838.
252 E. Katz, *ChemPhysChem*, 2019, **20**, 9.
253 Z. Guo, W. A. Johnston, J. Whitfield, P. Walden, Z. L. Cui, E. Wijker, S. Edwardraja, I. R. Lantadilla, F. Ely, C. Vickers, J. P. J. Ungerer and K. Alexandrov, *J. Am. Chem. Soc.*, 2019, **141**, 8128.
254 P. Bollella, M. Bellare, V. K. Kadambar, Z. Guo, K. Alexandrov, A. Melman and E. Katz, *ChemPhysChem*, 2020, **21**, 589.
255 A. Aviram, *J. Am. Chem. Soc.*, 1988, **110**, 5687.
256 S. Uchiyama, N. Kawai, A. P. de Silva and K. Iwai, *J. Am. Chem. Soc.*, 2004, **126**, 3032.
257 M. N. Win and C. D. Smolke, *Science*, 2008, **322**, 456.
258 D. P. Murale, H. Liew, Y. H. Suh and D. G. Churchill, *Anal. Methods*, 2013, **5**, 2650.
259 M. Prost and J. Hasserodt, *Chem. Commun.*, 2014, **50**, 14896.
260 R. Y. Tsien, *Am. J. Physiol.*, 1992, **263**, C723.
261 I. Takashima, R. Kawagoe, I. Hamachi and A. Ojida, *Chem. – Eur. J.*, 2015, **21**, 2038.
262 F. B. Yu, M. Gao, M. Li and L. X. Chen, *Biomaterials*, 2015, **63**, 93.
263 A. C. Sedgwick, H.-H. Han, J. E. Gardiner, S. D. Bull, X.-P. He and T. D. James, *Chem. Sci.*, 2018, **9**, 3672.
264 B. Finkler, I. Riemann, M. Vester, A. Grüter, F. Stracke and G. Jung, *Photochem. Photobiol. Sci.*, 2016, **15**, 1544.
265 J. B. Grimm, T. D. Gruber, G. Ortiz, T. A. Brown and L. D. Lavis, *Bioconjugate Chem.*, 2016, **27**, 474.

266 S. I. Reja, M. Gupta, N. Gupta, V. Bhalla, P. Ohri, G. Kaur and M. Kumar, *Chem. Commun.*, 2017, **53**, 3701.
267 A. P. de Silva, H. Q. N. Gunaratne, J.-L. Habib-Jiwan, C. P. McCoy, T. E. Rice and J.-P. Soumillion, *Angew. Chem., Int. Ed. Engl.*, 1995, **34**, 1728.
268 www.probes.com, see under; Lysosensor.
269 V. Goulle, A. Harriman and J.-M. Lehn, *J. Chem. Soc., Chem. Commun.*, 1993, 1034.
270 part vii.A. P. de Silva, A. Goligher, H. Q. N. Gunaratne and T. E. Rice, *ARKIVOC*, 2003, 229.
271 H. Maeda, H. Matsuno, M. Ushida, K. Katayama, K. Saeki and N. Itoh, *Angew. Chem., Int. Ed.*, 2005, **44**, 2922.
272 A. R. Lippert, G. C. Van De Bittner and C. J. Chang, *Acc. Chem. Res.*, 2011, **44**, 793.
273 Y. H. Hu, X. Gao, X. Li, H. Q. Liang, D. Zhang and C. L. Liu, *Sens. Actuators, B*, 2018, **262**, 144.
274 J.-Z. Li, Y.-H. Sun, C.-Y. Wang, Z.-Q. Guo, Y.-J. Shen and W.-H. Zhu, *Anal. Chem.*, 2019, **91**, 11946.
275 M. Kahan-Hanum, Y. Douek, R. Adar and E. Shapiro, *Sci. Rep.*, 2013, **3**, 1535.
276 J. Hemphill and A. Deiters, *J. Am. Chem. Soc.*, 2013, **135**, 10512.
277 B. Groves, Y.-J. Chen, C. Zurla, S. Pochekailov, J. L. Kirschman, P. J. Santangelo and G. Seelig, *Nat. Nanotechnol.*, 2015, **11**, 287.
278 J. Li, A. A. Green, H. Yan and C. H. Fan, *Nat. Chem.*, 2017, **9**, 1056.
279 C. C. Wu, S. Wan, W. J. Hou, L. Q. Zhang, J. H. Xu, C. Cui, Y. Y. Wang, J. Hu and W. H. Tan, *Chem. Commun.*, 2015, **51**, 3723.
280 S. M. Douglas, I. Bachelet and G. M. Church, *Science*, 2012, **335**, 831.
281 Y. Amir, E. Ben-Ishay, D. Levner, S. Ittah, A. Abu-Horowitz and I. Bachelet, *Nat. Nanotechnol.*, 2014, **9**, 353.
282 F. J. Isaacs, D. J. Dwyer, C. M. Ding, D. D. Pervouchine, C. R. Cantor and J. J. Collins, *Nat. Biotechnol.*, 2004, **22**, 841.
283 A. A. Green, P. A. Silver, J. J. Collins and P. Yin, *Cell*, 2014, **159**, 925.
284 A. A. Green, J. M. Kim, D. Ma, P. A. Silver, J. J. Collins and P. Yin, *Nature*, 2017, **548**, 117.
285 S. Matsuura, H. Ono, S. Kawasaki, Y. Kuang, Y. Fujita and H. Saito, *Nat. Commun.*, 2018, **9**, 4847.
286 J. E. Bronson, W. W. Mazur and V. W. Cornish, *Mol. BioSyst.*, 2008, **4**, 56.
287 H. N. Lin, W. M. Abida, R. T. Sauer and V. W. Cornish, *J. Am. Chem. Soc.*, 2000, **122**, 4247.
288 S. S. Gallagher, L. W. Miller and V. W. Cornish, *Anal. Biochem.*, 2007, **363**, 160.
289 J. J. Gao, P. D. Wu, A. Fernandez, J. M. Zhuang and S. Thayumanavan, *Angew. Chem., Int. Ed.*, 2020, **59**, 10456.
290 I. S. Turan, G. Gunaydin, S. Ayan and E. U. Akkaya, *Nat. Commun.*, 2018, **9**, 805.
291 A. Ojida, M. Mito-oka, K. Sada and I. Hamachi, *J. Am. Chem. Soc.*, 2004, **126**, 2454.